

no

Banded Whistlers Observed on OGO-4

by

Eugene M. Paymar

January 1972

Technical Report No. 3439-1

(NASA-CR-131495) ^{no} BANDED WHISTLERS
OBSERVED ON OGO-4 (Stanford Univ.) 53 p
HC \$4.75 CSCL 03B

N73-22079

Unclas
G3/07 17493

Prepared under

National Aeronautics and Space Administration
Grant NGR 05-020-288

RADIOSCIENCE LABORATORY
STANFORD ELECTRONICS LABORATORIES

STANFORD UNIVERSITY • STANFORD, CALIFORNIA



BANDED WHISTLERS OBSERVED ON OGO-4

by

Eugene M. Paymar

January 1972

Technical Report No. 3439-1

Prepared under
National Aeronautics and Space Administration
Grant NGR 05-020-288

Radioscience Laboratory
Stanford Electronics Laboratories
Stanford University Stanford, California

ABSTRACT

Inspection of broadband VLF records from the Stanford University/Stanford Research Institute experiment aboard OGO 4 shows that some whistlers exhibit a banded structure in which one or more bands of frequencies are missing from the whistler's spectrum. The phenomenon is commonly observed by satellites on midlatitude field lines at all local times and at various longitudes around the world. The dispersion of banded whistlers (BW) is of several tens of $\text{sec}^{1/2}$, indicating that they originated in the opposite hemisphere and are propagating downwards at the satellite. BW are generally spread in time (tenths of seconds) rather than sharply defined and tend to occur at random. The frequency spacing of the bands may be either uniform or irregular, and may vary radically between successive events. Several possible explanations for BW are considered. In particular, an analysis of the interaction of plane electromagnetic waves traveling in an anisotropic plasma with a field aligned slab of enhanced ionization is presented with promising results.

Preceding page blank

TABLE OF CONTENTS

	<u>Page</u>
I. INTRODUCTION	1
A. Introduction	1
B. Background	1
II. DATA	5
III. INTERPRETATION	17
A. Analysis of Potential Explanations	17
1. Instrumental Effects	17
2. Superposition of Multiple Signals	17
3. Banding in the Source Spectrum	21
4. Gyroresonance Interactions	22
5. Specular Reflection or Transmission	22
B. Computational Results	30
IV. DISCUSSION	40
APPENDIX	43
REFERENCES	45

LIST OF TABLES

<u>Table</u>	<u>Page</u>
1 Receiver Characteristics of Experiment D02	4

LIST OF ILLUSTRATIONS

<u>Figure</u>	<u>Page</u>
1 Frequency-time spectrogram of a banded whistler (BW) showing an unusually uniform banded structure	2
2 Frequency-time spectrograms illustrating three types of whistler fine structure	6
3 Frequency-time spectrogram of broadband data from OGO 4 showing many examples of banded whistlers	7
4 Histogram showing the occurrence of banded whistlers as a function of dipole latitude (Jensen-Cain model) over Orroral, Australia	9
5 Same data as preceding figure displayed as a function of L-value	10
6 OGO-4 calibration of band 2 receiver in magnetic mode at 10 kHz	12
7 Relative frequency response calibration of OGO-4 magnetic preamplifier	13
8 Comparison of OGO-4 band 2 and broadband receiver data at ~ 1452:40 UT on 3 October, 1967 over Orroral, Australia	14
9 Similar to Figure 8 except that the observations were made on the preceding pass at ~ 1315:30 UT	15
10 Data from Figure 8 calibrated from Figures 6 and 7 to show the spectral amplitude variation in the vicinity of the 2.5 kHz band in Figure 1	16
11 Tentative explanation of banding by multiple path propagation in the atmosphere	20
12 The geometry of the wave-slab interaction	24

LIST OF ILLUSTRATIONS (cont.)

<u>Figure</u>		<u>Page</u>
13	<u>Variation of the Minimum Value of the Transmission Coefficient, $\tau _{\min}^2$ (as defined in Eq. (19) in the text), with the incident wave normal angle, θ_I</u>	29
14	Sketch of refractive index surfaces μ_A and μ_B for media A and B respectively	31
15	Reflection spectrum	33
16	Computed transmission coefficients	36
17	Computed reflection coefficients	37
18	Two wave-slab interaction models--Model I appears to be usable on all 1-hop banded whistlers	39

ACKNOWLEDGMENTS

The author wishes to express his sincere gratitude to Professor Robert A. Helliwell for his guidance and patience. I am similarly indebted to Drs. J. J. Angerami and T. F. Bell for their deep interest, assistance and many stimulating discussions. I would also like to express appreciation to Drs. D. L. Carpenter and R. L. Smith for their encouragement and helpful criticism.

This research was supported by the National Aeronautics and Space Administration under grant NGR 05-020-288.

I. INTRODUCTION

A. INTRODUCTION

A detailed study of broadband very low frequency (VLF) whistler spectra reveals fine structure in virtually every case. Perhaps the most spectacular type of fine structure is the phenomenon of "banding" in which one or more bands of frequencies are missing from the whistler's spectrogram. A particularly striking example is shown in Figure 1. The objective of this report is to describe and explain observations of this phenomenon.

B. BACKGROUND

The surge of current which occurs during a lightning flash radiates a spectrum of electromagnetic energy which extends from a few Hertz up to around 20 MHz. The spectrum of these radiated waves generally peaks in the range 5-10 kHz. These waves may eventually enter the ionosphere and magnetosphere. At VLF frequencies the properties of the medium are such that the waves follow curved paths which are roughly aligned with the earth's magnetic field. Depending on the angle which the wave normal direction makes with the magnetic field the wave may also move in or out, to lower or higher L shells as it travels. At times such waves may become ducted (trapped by small field-aligned irregularities in the plasma density) and thus will more faithfully follow a particular field line. In addition the medium is dispersive so that different frequency components travel at different velocities. In the audio range this often results in the production at a receiver of a descending tone, called a "whistler."

Whistlers were first explained by Storey [1953]. Since then many publications on whistlers have appeared. For more details on the phenomenon

f
kHz
10 —

OGO 4 (ACT)
03 OCT 67

Reproduced from
best available copy.

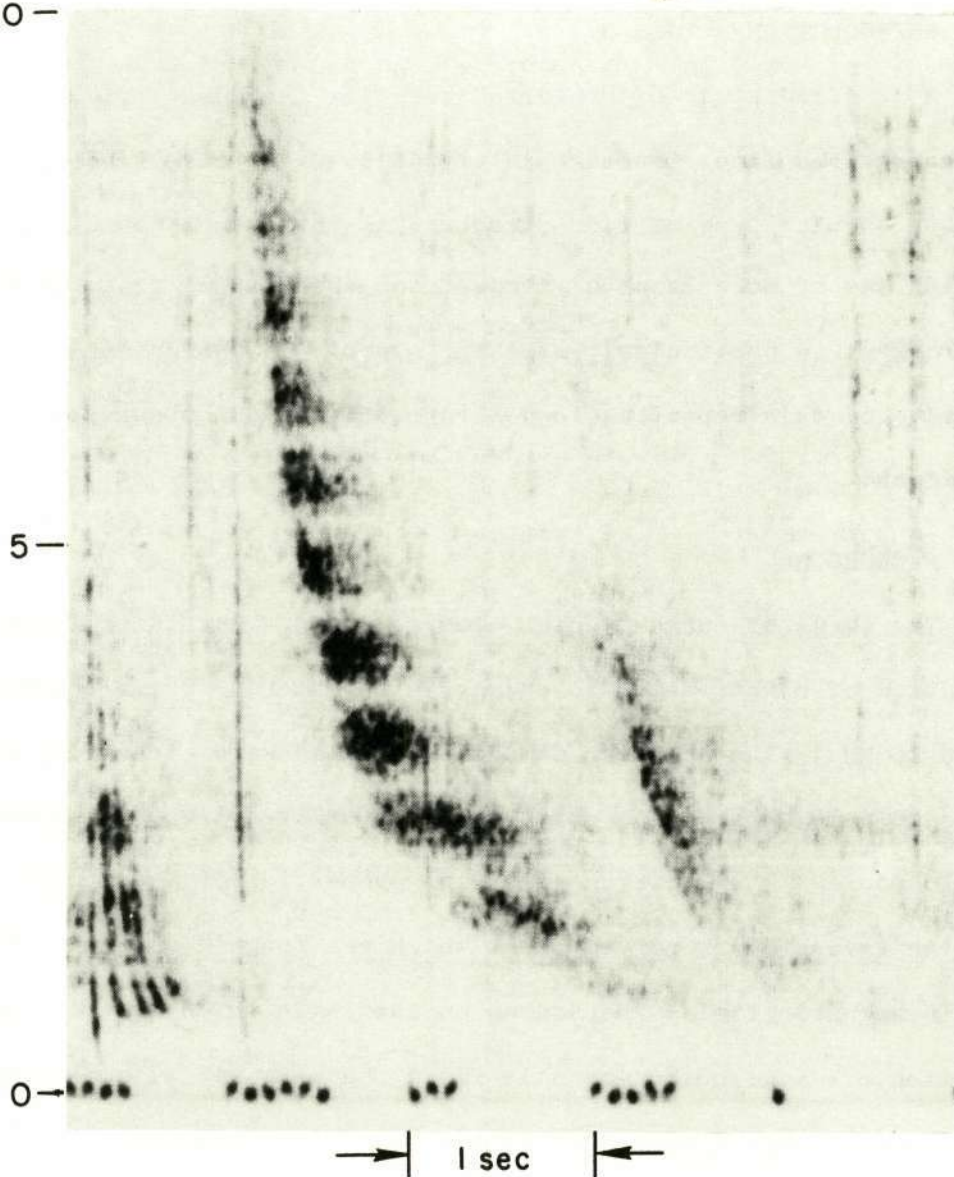


FIGURE 1. FREQUENCY-TIME SPECTROGRAM OF A BANDED WHISTLER (BW) SHOWING AN UNUSUALLY UNIFORM BANDED STRUCTURE. As usual, the dispersion of this event (of the order of $100 \text{ sec}^{1/2}$) indicates that it originated in the opposite hemisphere and is downgoing at the satellite. The relative darkness of the display measures the relative strengths of the received signals. The nulls in the spectrum of this banded whistler occur at odd half multiples of 810 Hz. The ephemeris indicates a proton gyrofrequency of 719 Hz and an invariant latitude $\Lambda = 51^\circ$ at the satellite. The local time is a few minutes after midnight. Also visible at the left of the record is an SP whistler which displays similar, but not identical banding.

see Helliwell [1965].

The earliest published examples of banded whistlers known to the author were from ground whistler data in Helliwell [1965]. However, examples of banded whistlers in the ground data are extremely rare. The present study concentrates on data obtained with the Stanford University/Stanford Research Institute VLF experiment flown on OGO 4, a low altitude polar orbiting satellite.

The Orbiting Geophysical Observatory, OGO 4, was launched on 28 July 1967 into a polar orbit with an inclination of 86° . The orbital period is around 100 minutes and the height varies from approximately 400 to 900 km. The satellite carries more than 20 different experiments. The data for this report were obtained from experiment DO2, the Stanford University/Stanford Research Institute VLF experiment.

Experiment DO2 consists of a 2.9 meter diameter loop antenna and a broadband preamplifier that drives three narrow band stepping receivers, two broadband receivers and one phase tracking receiver. The antenna was designed to be switchable on command so as to act as either an electric or magnetic field sensor. However, most of the data were obtained with the magnetic sensor because of a malfunction in the experiment. Table 1 describes the characteristics of the two receivers which provided data for this report. For a more detailed description of the experiment see Rorden et al [1966].

In Chapter 2 data from the above experiment which characterize the banded whistler phenomenon are presented. Chapter 3 will present some possible explanations, the most promising of which, spectral reflection or transmission from a field aligned slab of enhanced ionization, will be examined in detail. A summary, discussion, and suggestions for further research are presented in the final chapter.

SEL-71-054

TABLE 1. RECEIVER CHARACTERISTICS OF EXPERIMENT D02.

		Narrowbands				Broadbands	
		Band 1	Band 2	Band 3	Ph.Tracking	VLF	ELF
Frequency range (kHz)		0.2 - 1.6	1.6 - 12.5	12.5 - 100	14.4 - 26.3	0.3-12.5	0.015-0.300
Threshold Sensitivity	magnetic field ($\mu\gamma$)	32 - 4	6 - 0.8	1.2	1.6	8000-8	$10^5 - 10^3$
	electric potential at input of pre-amplifier (μV)	0.6 - 0.06	0.06	0.08	0.06	80	200.0 - 20
Dynamic range (db)		90	90	90	80	80	90
Local oscillator freq. (kHz)		3.16 - 4.53	25.33 - 36.25	202.5 - 290	23 - 34 and 2.7 - 3.6		
IF freq. (kHz)		2.97	23.75	190	8.2 and 5.0		
3-db bandwidth (Hz)		40	150	500	50		
ΔF /step (Hz/step)		5.4	43	344	100		
Data rate (kbit/sec)		4,16,64	4,16,64	4,16,64	4,16,64		
Sweep rate (steps/sec)		3.36,13.9,56	3.36,13.9,56	3.36,13.9,56			
Sweep time (sec/sweep)		73.4,18.4,4.6	73.4,18.4,4.6	73.4,18.4,4.6			
Integration time constant (msec)		460,114,20	146,40,9.4	48.4,18,4.4	32,8.6,2		

II. DATA

Broadband VLF spectra show a variety of fine structure, some of which are illustrated in Figure 2. Figure 2a shows a sharp well defined whistler which has gaps in its frequency spectrum. Close inspection of the data reveals such gapping in most well defined whistlers. A somewhat rarer phenomenon is illustrated in Figure 2b which shows a whistler having peaks of enhanced amplitude in its spectrum. This "beading" effect is no better understood than the spectrum gaps of Figure 2a. The fine structure of Figures 2a and 2b may be related to the banded whistlers. A third type of fine structure is illustrated in Figure 2c, where it is seen that the trace is composed of a collection of "blobs" rather than a single trace. These "blobs" are generally of a size much greater than the resolving limits of the spectrum analyzer. In this case the entity we call a "whistler" appears to consist of a collection of separate and distinct wave packets each with its own set of frequencies and propagation paths.

Banded whistlers (Figure 1 is a particularly outstanding example) are further illustrated in Figure 3, which shows six minutes of data taken over Ororral, Australia (ACT) on 30 May 1968. While Figure 1 shows a highly uniform spacing, this pass shows quite different behavior. For the whistler labeled "E", for example, the spacing between nulls ranges from 430 Hz to 1000 Hz. Also, little correlation is found from one banded whistler to the next. In "B" the spacing ranges from 300 to 500 Hz while 18 seconds later ("C") a relatively uniform spacing of approximately 1300 Hz occurs. Proton gyrofrequencies, deduced from the ephemeris, range smoothly from 693 Hz at "A" to 728 Hz at "B".

The phenomenon of banding occurs worldwide, having been detected at all receiving stations. Out of a sample of 87 passes one or more banded

OGO 4 JOB 16 DEC 67 ~1600 UT

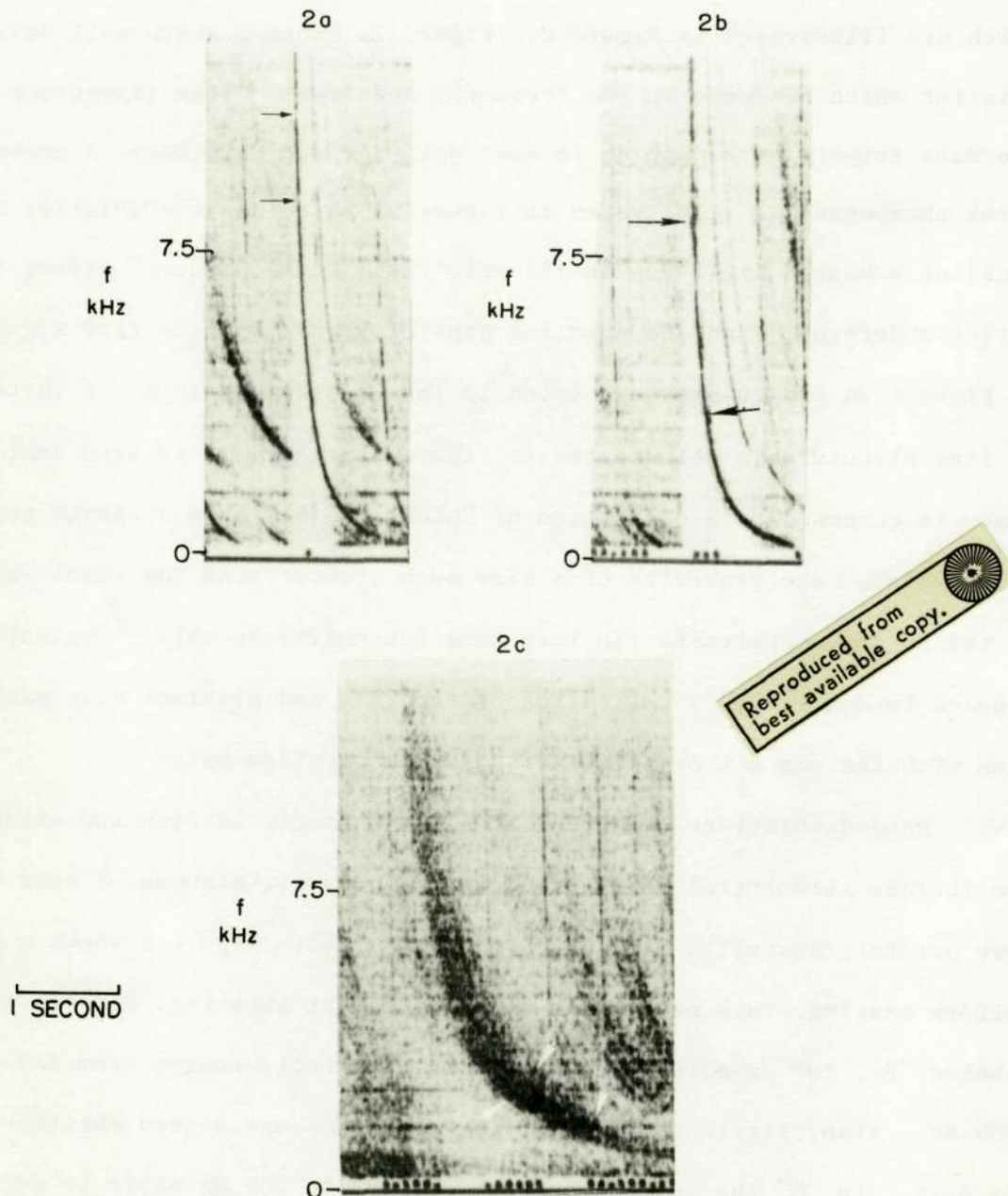


FIGURE 2. FREQUENCY-TIME SPECTROGRAMS ILLUSTRATING THREE TYPES OF WHISTLER FINE STRUCTURE. a) Shows a sharp, well defined whistler with two of the gaps in its spectrogram indicated by arrows. b) Shows a whistler having peaks of enhanced amplitudes. c) Shows a broadly dispersed whistler trace. The arrows indicate some of the small discrete elements of the whistler trace.

OGO 4 (ACT)
30 MAY 1968

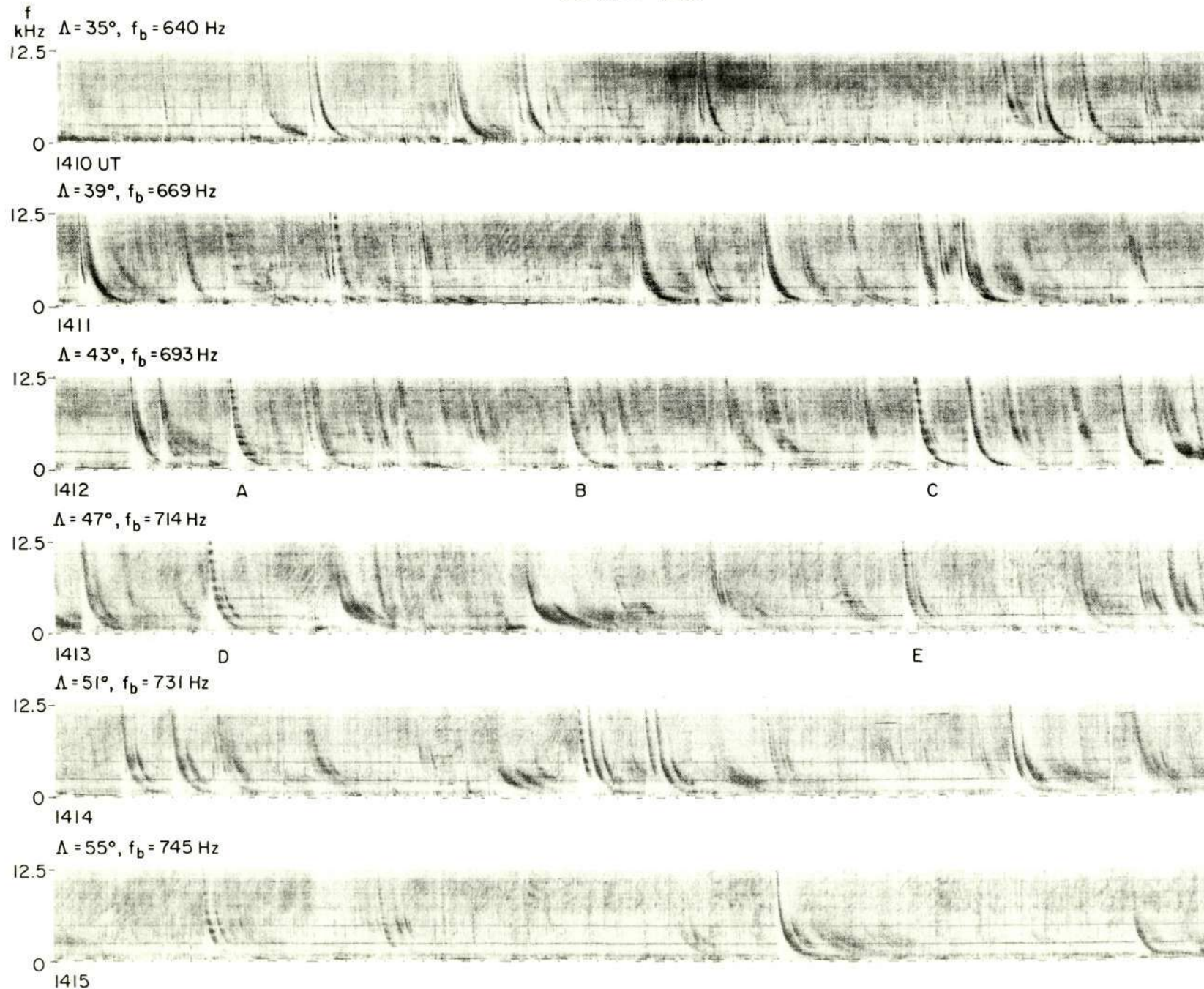


FIGURE 3. FREQUENCY-TIME SPECTROGRAM OF BROADBAND DATA FROM OGO 4 SHOWING MANY EXAMPLES OF BANDED WHISTLERS. Some of the more prominent examples are labeled "A" through "E".

whistlers occur on 70% of the nighttime passes. It occurs on 35% of the daytime passes, but this difference appears to be wholly attributable to the reduced overall whistler activity in daylight hours (i.e., on daytime passes there is at least an order of magnitude fewer whistlers than on nighttime passes--in fact often less than a dozen whistlers are detected per pass). Banded whistlers are well represented in those daytime passes which detect reasonably high levels of whistler activity.

At this point it is reasonable to ask "What is the distinction between the phenomena shown in Figures 2a and 2b and the banded whistlers?" At Stanford University our standard method of data presentation involves a 0-10 kHz or 0-13 kHz spectrogram displayed on a 3-cm wide roll of film. On this scale the phenomena shown in Figures 2a and b tend to be observable only on close inspection. By virtue of the number of nulls and/or the increased frequency width of the nulls, that subset of the data referred to as "banded whistlers" tend to be strikingly obvious to a casual observer. While this is admittedly a subjective distinction, it is operationally effective since the number of borderline cases is too small to significantly affect the statistics in the preceding and following paragraphs.

In addition to OGO 4 the phenomenon of banding has also been observed in this laboratory's data from OGO's 1, 2, and 3. Because of the availability of large quantities of data all statistics are based on OGO-4 data. Because of the high rate of banded whistler activity at ACT and the fact that ACT "sees" poleward beyond the plasmopause and to very low latitudes in the equatorial direction, more effort was spent analyzing data from this station than any other.

Figures 4 and 5 show the occurrence of banded whistler activity as a function of satellite dipole latitude and L value respectively. The high

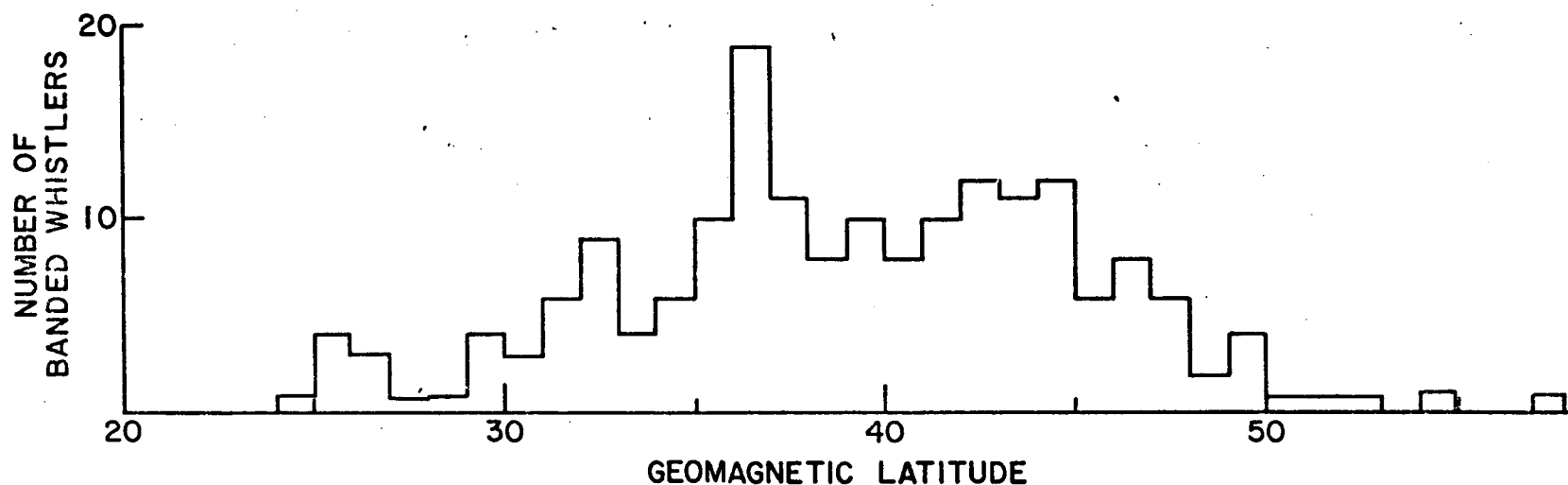


FIGURE 4. HISTOGRAM SHOWING THE OCCURRENCE OF BANDED WHISTLERS AS A FUNCTION OF DIPOLE LATITUDE (JENSEN-CAIN MODEL) OVER ORRORAL, AUSTRALIA. The data cover the periods September 1-3, 18-19, 1967, October 2-4, 1967 and May 26-30, 1968. These periods were selected because they each contain at least one pass with many well defined banded whistlers. Approximately 80% of these whistlers occurred at night. Data were generally received from the satellite beyond the upper and lower latitude cutoffs in the occurrence of banded whistlers.

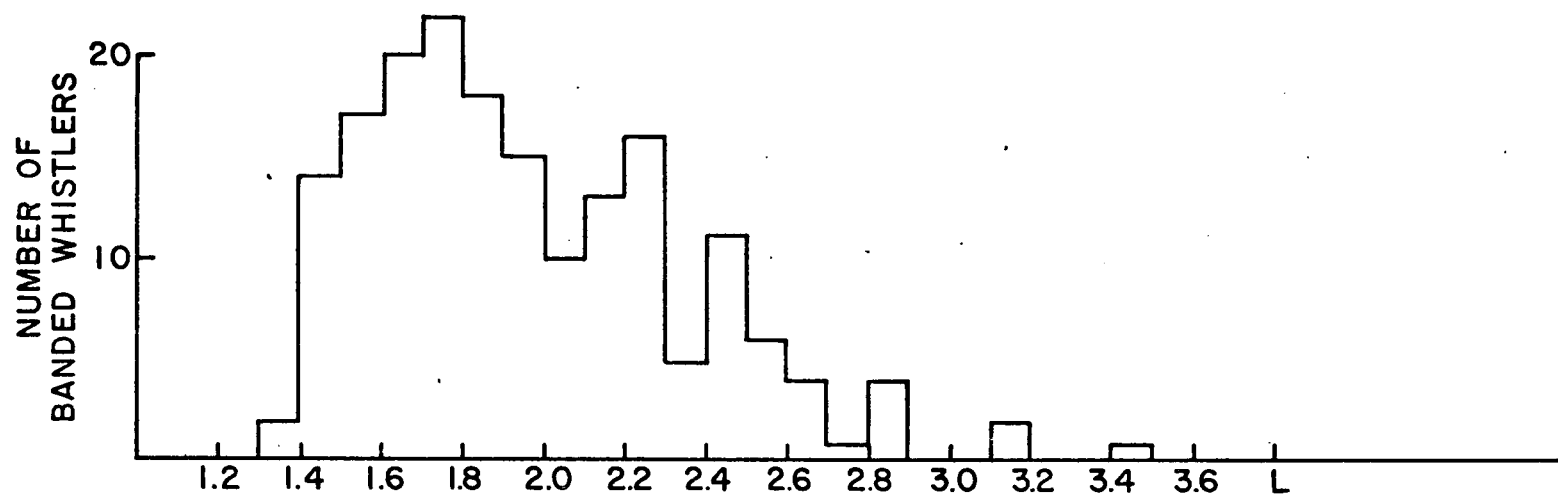


FIGURE 5. SAME DATA AS PRECEDING FIGURE DISPLAYED AS A FUNCTION OF L-VALUE.

latitude cutoff in these figures appears to coincide with the crossing of the plasmopause since banded whistler activity has been observed right up to the point where all whistler activity disappears. The low latitude cutoff at $\sim 30^\circ$ geomagnetic latitude appears to be real, although the sharpness of the cutoff in Figure 5 is rather misleading since, due to geometrical factors, the satellite spends greater amounts of time at the lower L shells. Data from the other stations are consistent with these latitude variations.

From records such as Figure 1 it is clear that severe attenuation of the signal has occurred in the nulls. The broadband receivers used on OGO 4 obtain their large ($\sim 60\text{db}$) dynamic range by log compressing and clipping the received signals. In order to accurately determine the amount of attenuation in the nulls it is necessary to use the data from the narrowband stepping receiver (calibrations are shown in Figures 6 and 7). The band-2 narrowband receiver sweeps upward in frequency at 43 Hz/step at a specified number of steps/second depending on groundbased command signals. It is rare for a well-defined null at some frequency in a banded whistler to occur just as the stepping receiver is scanning across that particular frequency. However, two clear examples have been found where the stepping receiver sweeps in frequency from a maximum to a null in a banded whistler. Figures 8 and 9 show the sweeping receiver data along with the corresponding banded whistlers. With the aid of the calibration charts Figure 10 was plotted showing the observed signal strength recorded by the sweeping receiver as the sweep moves into a null in the corresponding banded whistler. In both whistlers attenuations of $\sim 14\text{ db}$ were noted.

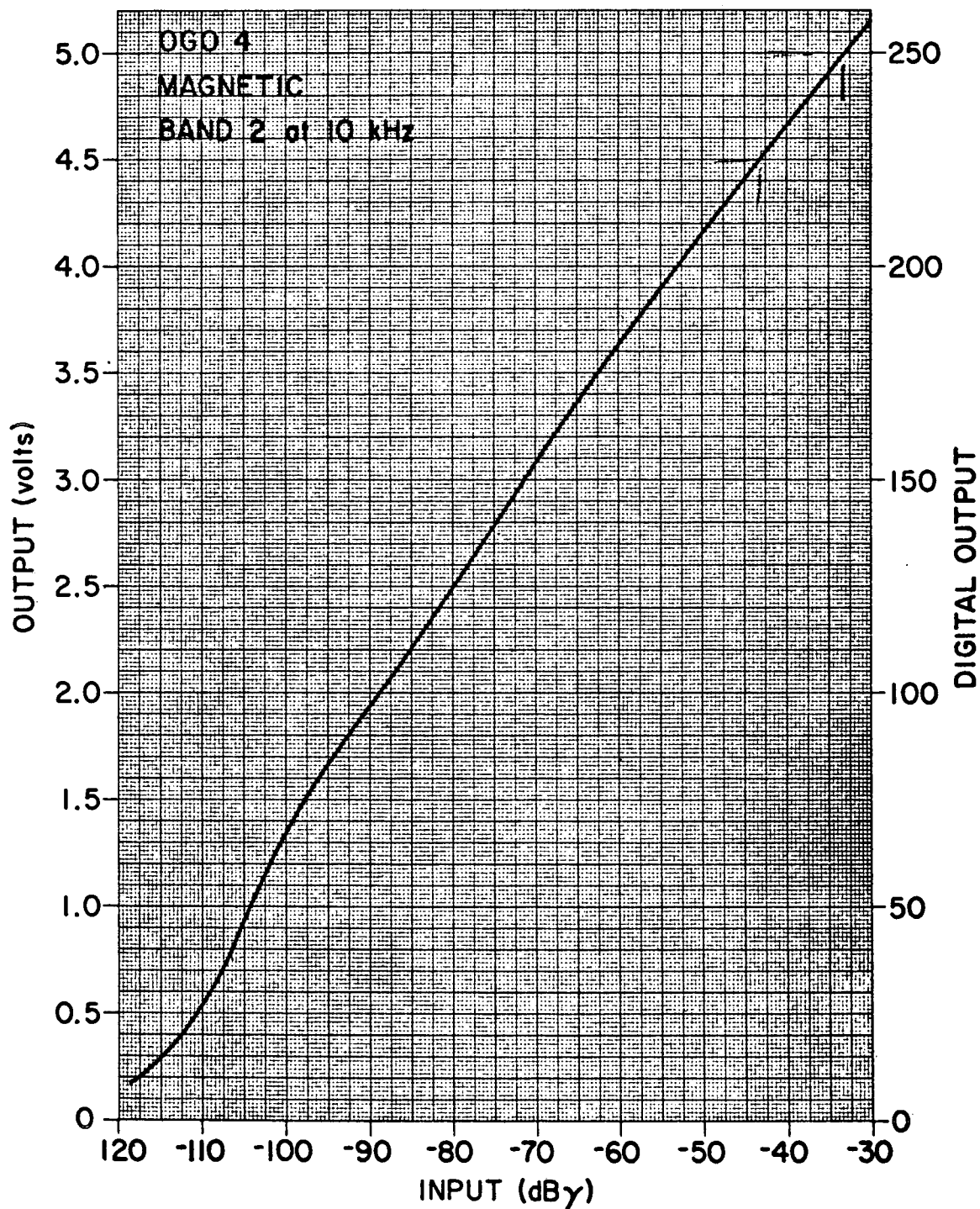


FIGURE 6. OGO-4 CALIBRATION OF BAND 2 RECEIVER IN MAGNETIC MODE AT 10 kHz. Use Figure 7 for calibration at other frequencies.

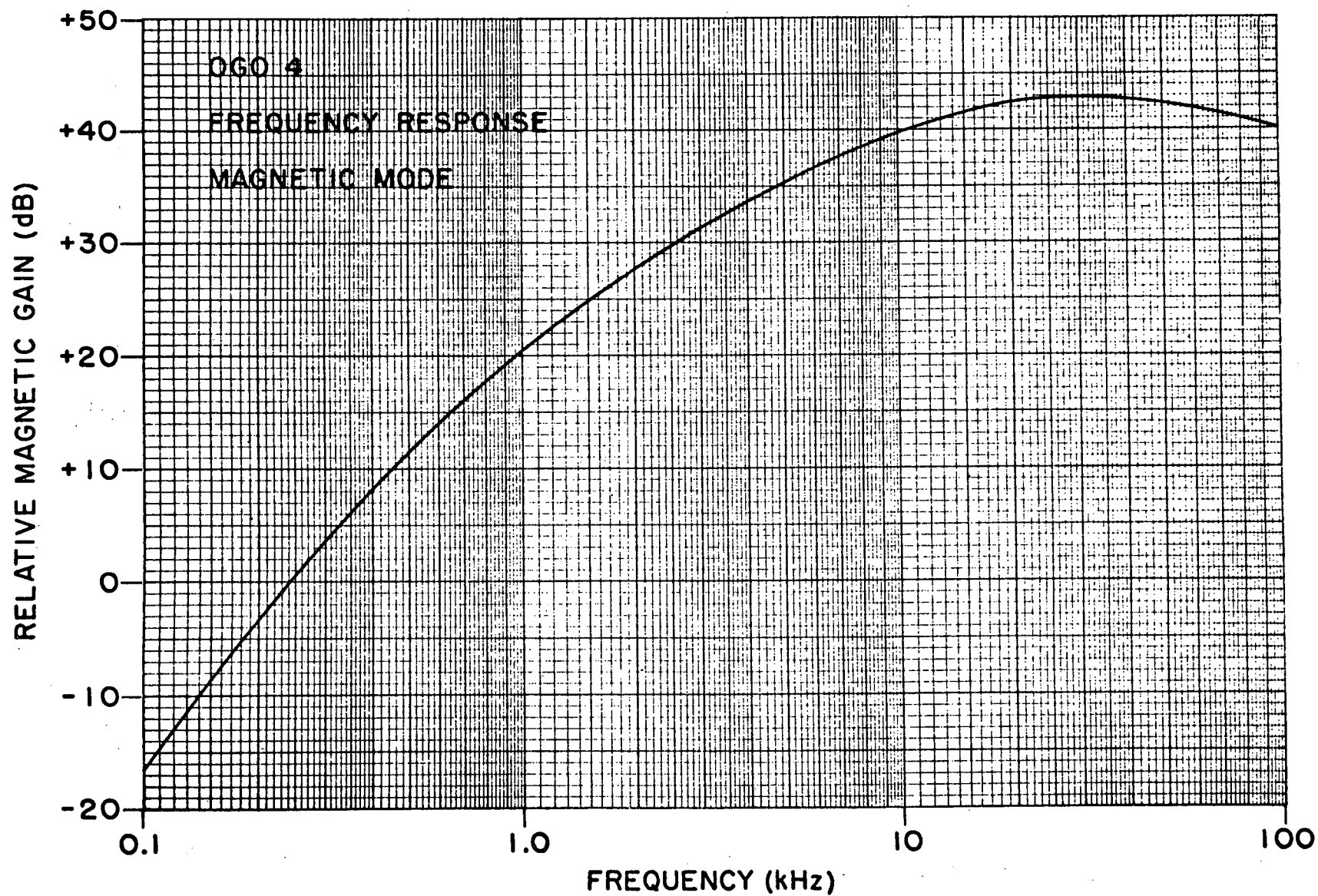


FIGURE 7. RELATIVE FREQUENCY RESPONSE CALIBRATION OF OGO-4 MAGNETIC PREAMPLIFIER.

Reproduced from
best available copy.

OGO 4 ACT 3 OCT 67

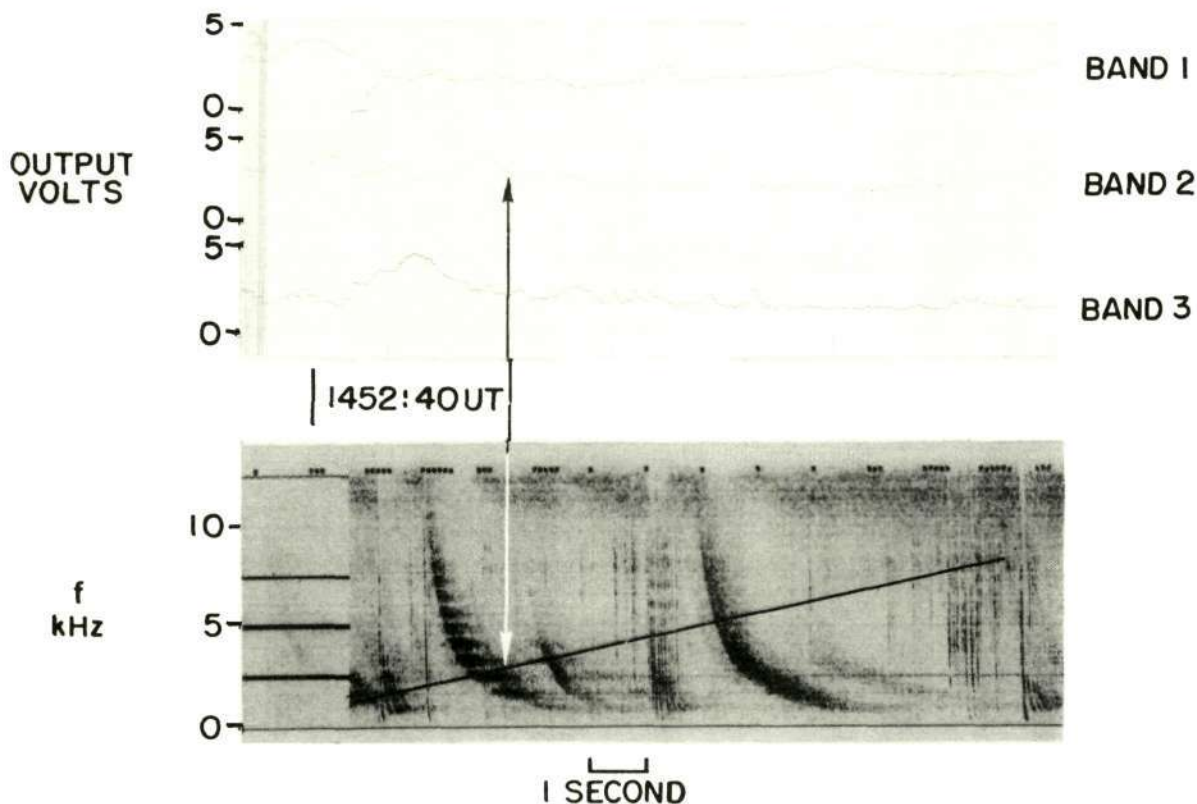


FIGURE 8. COMPARISON OF OGO-4 BAND 2 AND BROADBAND RECEIVER DATA AT
~ 1452:40 UT ON 3 OCTOBER, 1967 OVER ORRORAL, AUSTRALIA.

This record includes the data shown in Figure 1. The top graph shows the amplitude vs time variation of the signal received by the sweeping receivers. The Band 2 receiver has a 150 Hz (3 db) bandwidth and sweeps up in frequency at 43 Hz/step, 13.9 steps/second, repeating the sweep every 18.4 seconds. The bottom panel shows the frequency vs time spectrum of the data from the broadband receiver. The upward sloping straight line in this figure indicates the midfrequency being observed at any particular time by the Band 2 receiver. The time scales are the same on both panels.

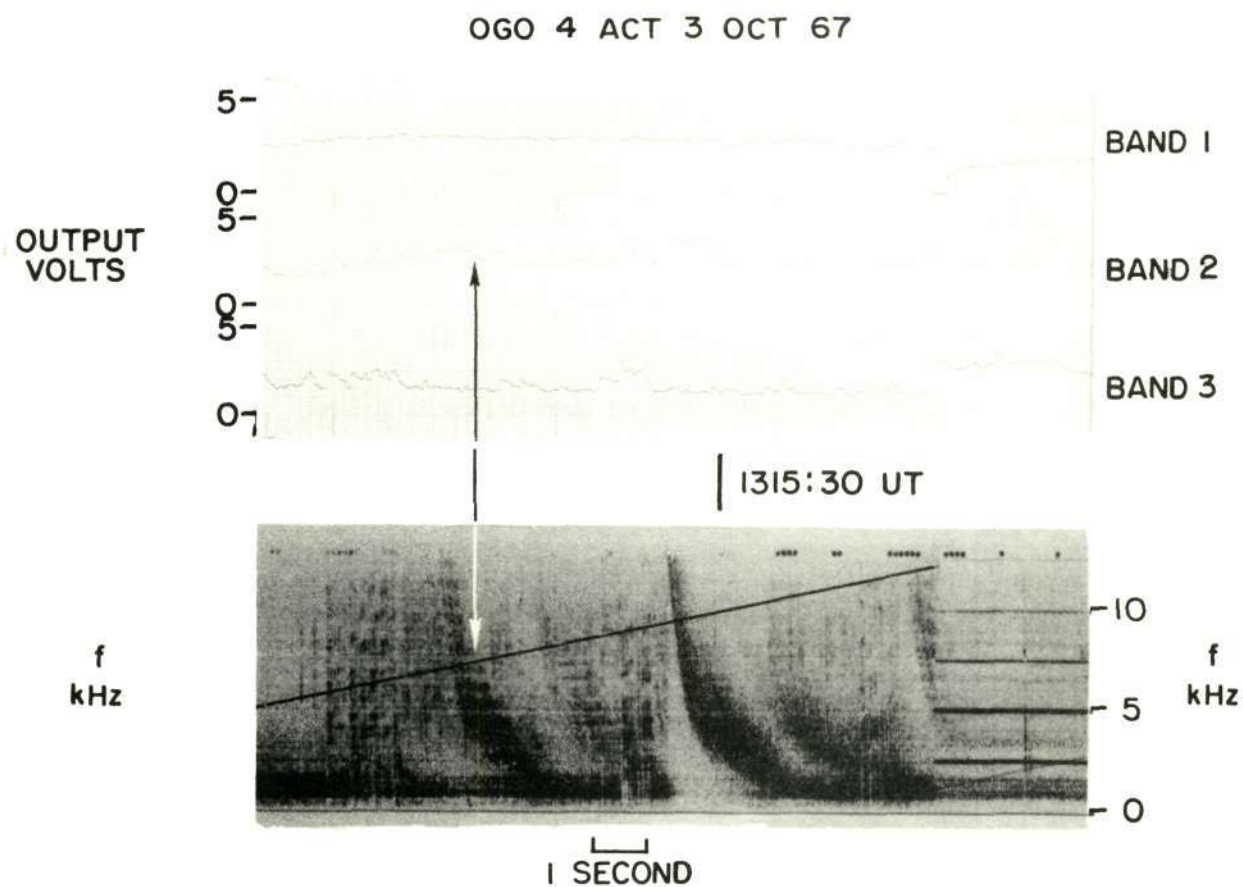


FIGURE 9. SIMILAR TO FIGURE 8 EXCEPT THAT THE OBSERVATIONS WERE MADE ON THE PRECEDING PASS AT $\sim 1315:30$ UT.

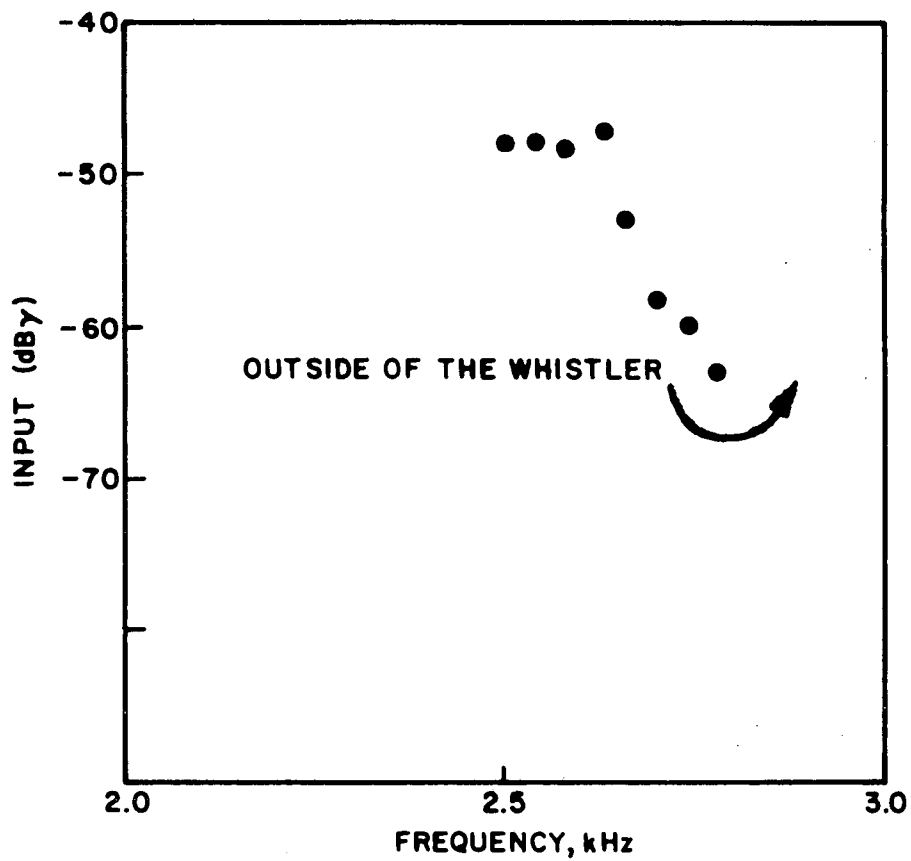


FIGURE 10. DATA FROM FIGURE 8 CALIBRATED FROM FIGURES 6 and 7 TO SHOW THE SPECTRAL AMPLITUDE VARIATION IN THE VICINITY OF THE 2.5 kHz BAND IN FIGURE 1.

III. INTERPRETATION

A number of potential explanations for the banded whistlers can be advanced. The merits of eight models are discussed in this chapter. They fall roughly into the following five categories: 1) instrumental effects; 2) superposition of multiple signals; 3) banding in the source spectrum; 4) gyroresonance interactions; and 5) specular reflection or transmission.

A. ANALYSIS OF POTENTIAL EXPLANATIONS

1. Instrumental Effects

It is, of course, necessary first to deal with the possibility that the phenomenon is spurious. Potential sources of instrumental effects are a) the satellite; b) the receiving station, c) the processing at Goddard Space Flight Center, and d) our Rayspan spectrum analyzer.

The occurrence of the phenomenon on other satellites (e.g., OGO 2, T. Bell, private communication) and all ground receiving stations argues against (a) or (b). The apparent latitude effects noted in Figures 4 and 5 argue very strongly against (b), (c), or (d) and to a lesser extent, (a). The possibility that non-uniform response of the Rayspan filters is responsible for the phenomenon is unreasonable in view of the randomness of the frequencies at which the nulls occur. This source was further checked by comparing the same data on 0-10 kHz and 0-13 kHz records. The Rayspan (spurious) lines remained fixed while the nulls moved to their new positions, as expected. Finally, ground whistler data processed on the same Rayspan analyzer have only rarely contained any banded whistlers.

2. Superposition of Multiple Signals

Multiple stroke. Given that the effect is real, one possibility is that the nulls are caused by destructive interference of signals from multiple stroke lightning. Assuming lightning to be impulsive the total signal $V(t)$ is given by

$$V(t) = V_1 \delta(t-t_1) + V_2 \delta(t-t_2) \quad (1)$$

The Fourier spectrum of $V(t)$ is given by

$$V(\omega) = \int_{-\infty}^{\infty} V(t) e^{-i\omega t} dt = V_1 e^{-i\omega t_1} + V_2 e^{-i\omega t_2} \quad (2)$$

The amplitude of the spectrum is given by

$$|\tilde{V}(\omega)|^2 = |V_1|^2 + |V_2|^2 + 2V_1 V_2 \cos \omega (t_2 - t_1) \quad (3)$$

Examination of Eq. (3) shows that $|V(\omega)|^2$ varies sinusoidally between the values $(V_1 + V_2)^2$ and $(V_1 - V_2)^2$. Shaw and Gurnett [1971] used this model with $V_1 = V_2$ and $t_2 - t_1 = \Delta t$ to explain some banding of whistlers observed on Injun 5. Their observations were made in the range 0 - 500 Hz and the spacings between bands typically ranged from 10 to 30 Hz. These spacings correspond to a Δt on the order of 50 milliseconds. Uman [1969] reports maximum and minimum values (used in the sense that most values fall between these limits) for Δt of 100 and 3 milliseconds, respectively with representative values of ~ 40 milliseconds. The latter value fits Shaw and Gurnett's data and model very well, but the lower value is not sufficient to explain whistler "C" in Figure 3 which has a spacing of ~ 1300 Hz. A more serious objection is raised if one notes (as in Figure 3) that the spacing between nulls in the same banded whistler is often non-uniform. Furthermore, even among whistlers with uniform spacing (e.g., Figure 1), the nulls are

usually either much narrower than the maxima or vice-versa. However this model, based on Eq. (1), predicts a simple sinusoidal variation of amplitude with frequency rather than the spectral shapes noted above. For a discussion of the effects of substituting a more realistic model for the time behavior of a lightning stroke into Eq. (1) see the second paragraph in section on different paths within the ionosphere below.

Lightning strokes from different locations. We can escape entirely the first objection raised above by assuming that the two strokes are not coming from the same lightning channel, but rather occur in different locations separated by a distance large enough to produce the observed range of frequency spacings. However, this model has precisely the same difficulty as the preceding one in terms of reproducing the observed spectral shapes.

Different paths in the waveguide. A very similar tentative explanation is illustrated in Figure 11. There, one of the waves radiated by the lightning stroke travels directly to the entry point into the ionosphere while the other first reflects off the earth and hence travels a longer path. However, a $\Delta f \sim 1 \text{ kHz}$ implies a travel time differential of ~ 1 millisecond corresponding to a path difference of ~ 300 kilometers. It is clear that the path differential maximizes when the entry point is directly above the source. Since the entry point is $\sim 80 - 100 \text{ km}$ above the earth's surface, not one, but several hops will be required. However, absorption and reflection losses would then make the multi-hop wave amplitude too small to cancel the direct wave to the extent shown in Figure 10. In addition this model is clearly no better able to reproduce the observed spectral shapes than the two preceding ones.

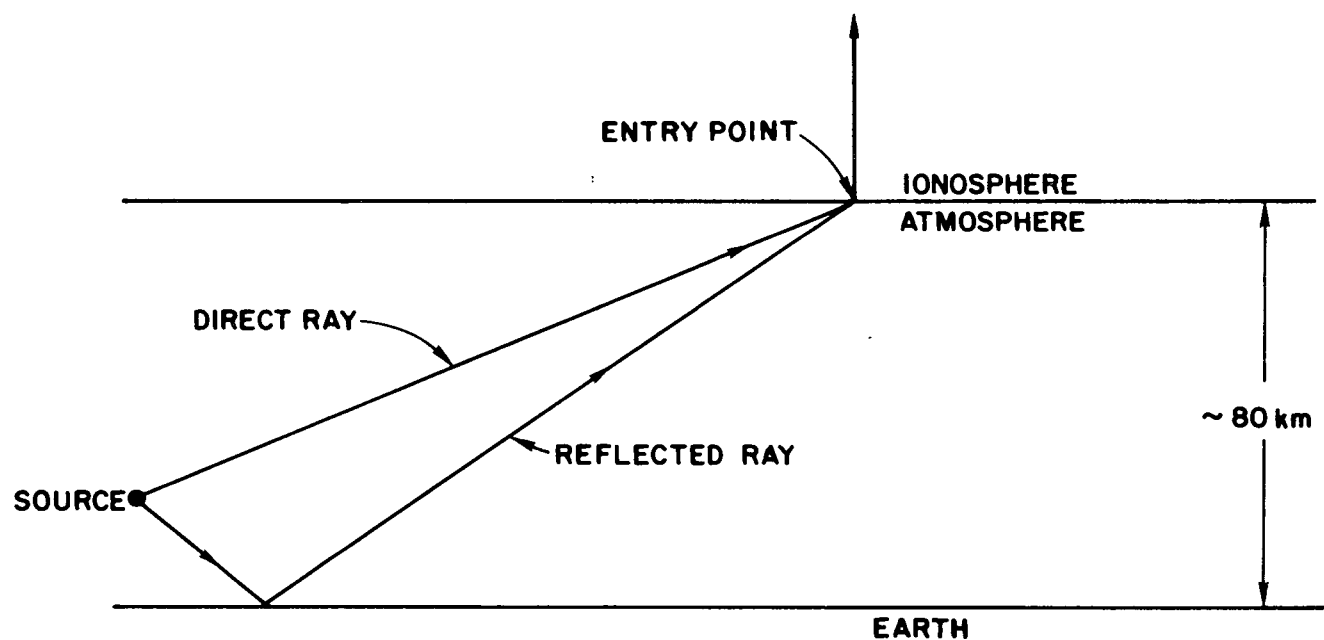


FIGURE 11. TENTATIVE EXPLANATION OF BANDING BY MULTIPLE PATH PROPAGATION IN THE ATMOSPHERE.

The first path is a direct ray from the originating lightning source through the atmosphere to an entry point into the ionosphere. The second ray reflects off the earth's surface while traveling between the same two end points. Higher order paths involving reflections off the ionosphere as well as the earth are also possible. For clarity the drawing is not to scale.

Different paths within the ionosphere. The last possibility along the previous lines is that the nulls arise due to the superposition of two waves that have traveled different paths within the ionosphere. However, let us note (as, for example, in Figure 1) that the nulls may continue to be observed at a constant frequency for times on the order of a second. The diffuseness of these whistlers is attributed to multiple entry points into the ionosphere thereby implying multiple paths to the satellite, which is traveling at 7 km/sec. The phase-path integrals vary significantly along the paths, and it is unreasonable to expect that the same relative phase relationships will be maintained over a 7 km interval. Of course, this argument also applies to the two preceding models since Δt (and thus Δf) will depend on the location of the entry point into the ionosphere in these two models.

These explanations cannot be salvaged by assuming more realistic models for the time behavior of the lightning stroke in Eq. (1). Uman [1969] reports that the time duration (t_s) of a stroke is $\sim 20 - 60 \mu\text{sec}$. Thus variations in a lightning pulse take place on a time scale $\leq t_s$. It may then be shown by arguments similar to those on page 18 that these variations in the time domain produce spectral components which vary less rapidly than $\cos 2\pi f t_s$. That is, t_s would have to be one to two orders of magnitude larger than the accepted values to produce minima spaced as closely as those in the banded whistlers.

3. Banding in the Source Spectrum

However, if such large times, t_s , did actually exist, then we are saying in effect that the nulls arise from holes within the lightning source spectrum. If, indeed the sources were involved, then the same patterns should appear with similar regularity in the ground whistler

data. In fact, banding in the ground data appears, but only very rarely, and few examples have been found to date.

4. Gyroresonance Interactions

The first few examples of banded whistlers noted by the author all had very uniform spacings. This immediately led to speculation that some type of gyroresonance interaction was involved. The existence of such interactions in the ionosphere was reported by Gurnett and Mosier [1969]. They found attenuation bands in auroral zone noise at integer multiples of the local proton gyrofrequency. However, in Figure 1 the nulls occur at odd half multiples of 810 Hz (± 30 Hz) rather than at integer multiples of the local proton gyrofrequency of 719 Hz. Also in Figure 3 the local proton gyrofrequencies range from 693 Hz at whistler "A" up to 728 Hz at whistler "E". Spacings observed in the latter whistler range from 430 Hz to 1000 Hz and little correlation seems to exist from one banded whistler to the next. For example, at "B" the spacing ranges from 300 Hz to 500 Hz while 18 seconds later at "C" a relatively uniform spacing of ~ 1300 Hz occurs. Therefore theories of ion gyroresonance interactions are not adequate to explain these observations.

5. Specular Reflection or Transmission

The last model to be discussed in this report involves specular transmission or reflection of an incident plane wave from a slab of enhanced ionization aligned parallel to the earth's magnetic field \vec{B}_0 and extending in the E-W direction. Without loss of generality, \vec{B}_0 is taken to be along the x-axis. The x-z plane is taken to be the earth's meridian plane, and the incident wave normal \vec{k} is assumed to be in this plane. This is a common assumption, and as Thorne [1969] has pointed out, the medium has a tendency to focus \vec{k} back onto the meridian plane if

the initial direction of \vec{k} is not in this plane. Figure 12 shows the geometry.

Define: \vec{E}_I = incident electric field strength,
 \vec{E}_R = reflected electric field strength,
 \vec{E}_T = transmitted electric field strength,
 \vec{E}_+ = electric field of the upgoing wave in the slab
 \vec{E}_- = electric field of the downgoing wave in the slab
 \vec{k}_i = wave normal vector in region i
 k is related to the wave frequency ω and the refractive index μ in the region by
 $|k| = \frac{\omega}{c} |\mu|$ where c is the velocity of light.
 \vec{E}_n = electric field component in \vec{k} direction
 \vec{E}_\perp = electric field component in $\vec{B}_0 \times \vec{k}(-y)$ direction
 \vec{E}_\parallel = electric field component in $\vec{E} \times \vec{k}$ direction
 L = thickness of the slab.

The boundary conditions are that the components of electric field parallel to a dielectric boundary are continuous across that boundary (see for example, Ramo et al., [1965]). Thus the conditions at the lower surface (assumed to be $z = 0$) are:

$$E_{XI} + E_{XR} = E_{X+} + E_{X-} \quad (4)$$

$$E_{YI} + E_{YR} = E_{Y+} + E_{Y-} \quad (5)$$

The boundary conditions at the surface $z = L$ are:

$$E_{XT} = e^{ik_{zB}L} E_{X+} + e^{-ik_{zB}L} E_{X-} \quad (6)$$

$$E_{YT} = e^{ik_{zB}L} E_{Y+} + e^{-ik_{zB}L} E_{Y-} \quad (7)$$

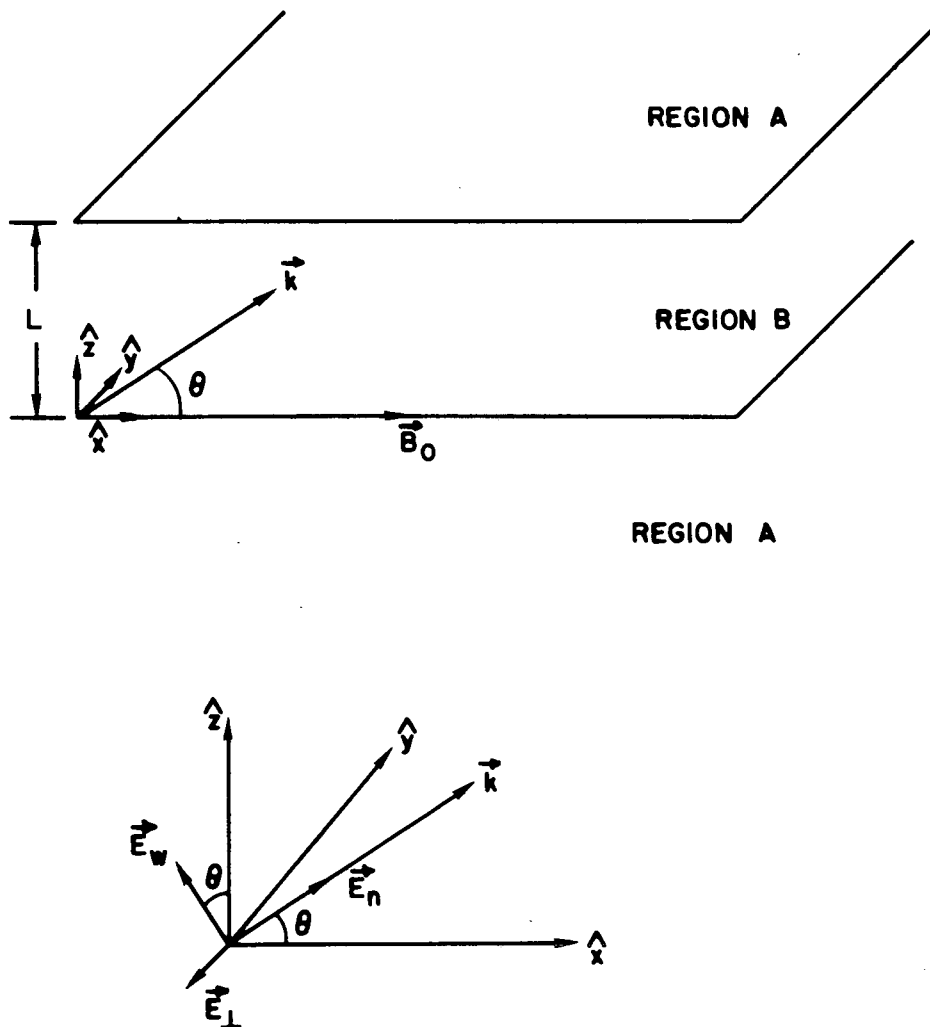


FIGURE 12. THE GEOMETRY OF THE WAVE-SLAB INTERACTION.

In the upper figure, region A is the ambient plasma. Region B is a slab of thickness L whose density is enhanced by a factor δ over that of the ambient plasma. The earth's magnetic field \vec{B}_0 is in the \hat{x} direction, parallel to the slab. The wave normal vector \vec{k} lies in the plane formed by \hat{x} and the slab normal direction, \hat{z} . It makes an angle θ with \vec{B}_0 . The lower figure shows the three principal electric field axis of the wave, \vec{E}_n (parallel to \vec{k}), \vec{E}_\perp (in the $-\hat{y}$ direction), and \vec{E}_w (in the $\vec{E}_\perp \times \vec{E}_n$ direction).

Following Smith and Brice [1964]

$$\begin{aligned}\mu_p^2 &= 1 - \sum_r \frac{X_r}{pY_r + 1} \quad p = \pm 1, 0 \\ W_p^2 &= \mu_p^{-2} \\ W_e^2 &= \frac{1}{2} (W_1^2 + W_{-1}^2) \\ 2W^2 &= 2W_e^2 + (W_o^2 - W_e^2) \sin^2 \theta \pm [(W_e^2 - W_o^2)^2 \sin^4 \theta + (W_1^2 - W_{-1}^2)^2 \cos^2 \theta]^{1/2} \quad (8)\end{aligned}$$

where

μ = refractive index

$W = 1/\mu$

θ = angle between \vec{k} and \vec{B}_o

$k_{zB} = k \sin \theta$ evaluated in the slab

\sum_r = sum over all types of charged particles in the plasma

$X_r = f_{or}^2 / f^2$

$Y_r = f_{Hr} / f$

f = wave frequency

$f_{Hr} = \text{gyrofrequency of } r^{\text{th}} \text{ type particle} = \frac{|\vec{B}_o| q_r}{2\pi m_r}$

$f_{or} = \text{plasma frequency of } r^{\text{th}} \text{ type particle} = \left[\frac{N_r q_r^2}{\epsilon_o M_r} \right]^{1/2} \frac{1}{2\pi}$

ϵ_o = dielectric constant of free space =

q_r, m_r, N_r are respectively the (signed) charge, mass, and number density of the r^{th} type particle.

(rationalized MKS units used throughout)

Note that

$$\frac{E_x}{E_y} = \frac{E_n}{E_y} \cos \theta - \frac{E_w}{E_y} \sin \theta \stackrel{\text{def}}{=} Q$$

Following Smith's class notes [1968]:

$$E_w : E_n : E_{\perp} = W^2 (W_e^2 - W^2) : - (W_e^2 - W^2) (W_o^2 - W^2) \tan \theta : i W^2 (W_1^2 - W_{-1}^2) \frac{\cos \theta}{2} \quad (9)$$

Noting that $E_y = -E_{\perp}$ we have

$$Q = \frac{-(w_e^2 - w^2)(w_o^2 - w^2) \tan \theta \cos \theta - w^2(w_e^2 - w^2) \sin \theta}{-i w^2(w_1^2 - w_{-1}^2) \frac{\cos \theta}{2}} = -2i \frac{\tan \theta (w_e^2 - w^2) w_o^2}{(w_1^2 - w_{-1}^2) w^2} \quad (10)$$

There is of course a different value of Q for each region and Q changes sign with θ . Equations (4) and (6) transform to

$$Q_A (E_{YI} - E_{YR}) = Q_B (E_{Y+} - E_{Y-}) \quad (4')$$

$$Q_A E_{YT} = Q_B (e^{ik_{zB}L} E_{Y+} - e^{-ik_{zB}L} E_{Y-}), \quad (6')$$

where the Q 's are computed for the positive values of θ .

Using Eqs. (5) and (7) to eliminate E_{Y+} and E_{Y-}

$$E_{YT} e^{-ik_{zB}L} (1 + \gamma) - E_{YR} (1 - \gamma) = E_{YI} (1 + \gamma) \quad (11)$$

$$E_{YT} e^{+ik_{zB}L} (1 - \gamma) - E_{YR} (1 + \gamma) = E_{YI} (1 - \gamma) \quad (12)$$

where

$$\gamma = Q_A / Q_B.$$

Now eliminating E_{YR} yields:

$$\tau \stackrel{\text{def}}{=} E_{YT} / E_{YI} = \frac{2\gamma}{2\gamma \cos k_{zB}L - i(1 + \gamma^2) \sin k_{zB}L} \quad (13)$$

Assuming no losses in the plasma (k_{zB} and γ are real) then the fraction of the wave energy transmitted through the slab (i.e., the transmission coefficient) is given by

$$|\tau|^2 = \frac{4\gamma^2}{4\gamma^2 \cos^2 k_{zB}L + (1 + \gamma^2)^2 \sin^2(k_{zB}L)} = \frac{4\gamma^2}{4\gamma^2 + (1 - \gamma^2)^2 \sin^2(k_{zB}L)} \quad (14)$$

Under this assumption the reflection coefficient $|\rho|^2 \stackrel{\text{def}}{=} |E_{YR}/E_{YI}|^2$ satisfies

$$|\rho|^2 + |\tau|^2 = 1 \quad (15)$$

Equation (14) requires knowledge of the value of the refractive index μ_B and $W_B^2 (= \mu_B^{-2})$. In order to obtain this information Eq. (8) must be combined with Snell's law:

$$\mu_A \cos \theta_A = \mu_B \cos \theta_B$$

which may also be written

$$\cos^2 \theta_B = \alpha W_B^2 \quad (16)$$

where:

$$\alpha = \cos^2 \theta_A / W_A^2 \quad (17)$$

Using Eq. (16) to eliminate θ_B from Eq. (8) we obtain the following quadratic expression in W_B^2

$$(1 - \alpha W_e^2 + \alpha W_o^2) W_B^4 + (\alpha W_{-1}^2 W_{-1}^2 - \alpha W_e^2 W_o^2 - W_o^2 - W_e^2) W_B^2 + W_e^2 W_o^2 = 0 \quad (18)$$

where all quantities (except α) are evaluated inside the slab. Equation (18) (a particular form of Booker's quartic) is solved for the fast mode (i.e., choose the '+' sign in the solution) and then θ_B is determined with the aid of Eqs. (16) and (17). θ_A , the slab thickness (L), and the quantities which determine W_{-1} , W_o and W_e (ion mass, f_p , and f_H) are all parameters. They are not necessarily independent. For example if one specifies an altitude within the latitude range of occurrence of the banded whistlers this not only tends to specify the ions, f_p , and f_H , but it may also, depending on one's model for slab formation, determine L.

To determine the transmission coefficients as a function of frequency a FORTRAN program (see Appendix) was written for use on Stanford University's IBM 360/67 computer. Several assumed models of slab thickness and altitude location were tried. These were combined with three different types of models for the variation of the incident wave normal angle, θ , with frequency.

Before discussing these models let us note some of the properties of Eq. (14). This equation is deceptively simple and masks some rather complex physical and mathematical behavior. Calculations indicate that γ varies much more slowly than $\sin k_{zB}L$ as f changes. To a good approximation the minimum values of Eq. (14) with respect to f are given by

$$|\tau|_{\min}^2 \equiv \frac{4\gamma^2}{(1 + \gamma^2)^2} \quad (19)$$

This quantity is plotted in Figure 13 as a function of the incident wave normal angle θ_I . As expected it goes to zero at zero wave normal angle since the wave is then traveling parallel to the slab. As the wave normal angle increases, more and more energy is directed into the slab. However, at the same time the impedance mismatch between the two media starts to grow as the difference in refractive indices increases. Thus, it is not unreasonable to expect that at some point the latter effect might counter balance the former and $|\tau|_{\min}^2$ would reach a peak.

The slab also has two other interesting properties. However, we must first distinguish between the three cases illustrated in Figure 14. Figure 14a sketches the closed wave normal surfaces for regions A and B characteristic of frequencies below the lower hybrid resonance (LHR). The approximate expression for the LHR frequency was given by Brice and

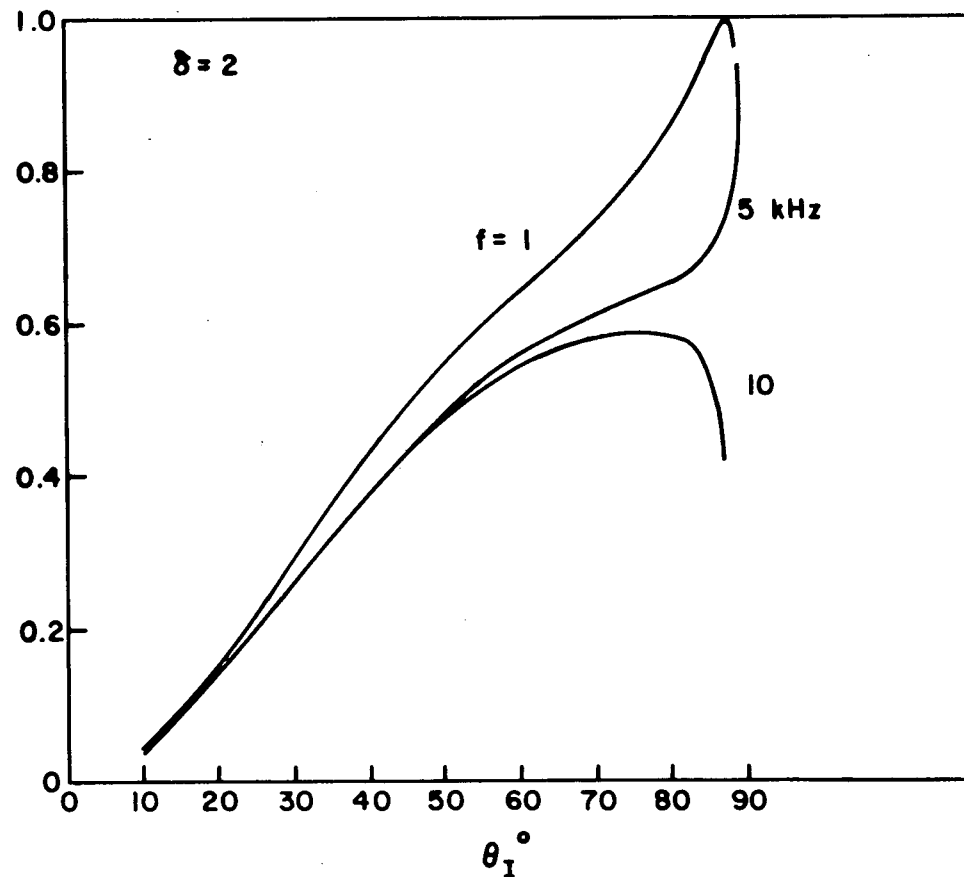
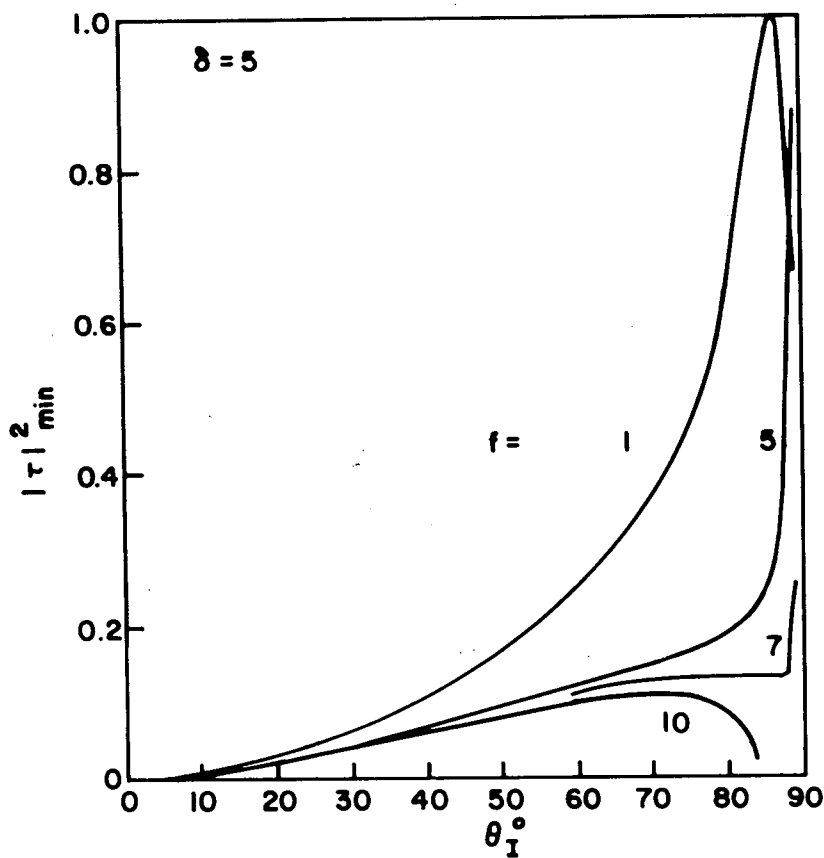


FIGURE 13. VARIATION OF THE MINIMUM VALUE OF THE TRANSMISSION COEFFICIENT, $|\tau|_{\min}^2$ (AS DEFINED IN EQ. (19) IN THE TEXT), WITH THE INCIDENT WAVE NORMAL ANGLE, θ_I . The graphs are parameterized by the wave frequency f in kiloHertz. The following parameters for the ambient medium (A) were used in the calculations: plasma frequency $f_{oe} = 3.2$ MHz, electron gyrofrequency $f_{He} = 1.3$ MHz and ionic composition 100% O^+ , leading to a lower hybrid resonance at 7.03 kHz. The left graph corresponds to an enhancement factor $\delta = 5$ and the right one to $\delta = 2$.

and Smith [1965] as:

$$f_{\text{LHR}} = \left[\frac{1}{M} \frac{f_o^2 + f_H^2}{f_o^2 + f_H^2} \right]^{1/2} \quad (20)$$

where M is the ion to electron mass ratio of the single ion (O^+) assumed in this model. Since we are dealing with a slab of enhanced ionization it is obvious that there will be a range of frequencies that lie above the LHR frequency for region A and below that for region B. In this range the refractive index surfaces will appear as shown in Figure 14b. Above this range both surfaces open up as shown in Figure 14c. It is interesting to note in the latter two cases that the two surfaces cross.

Figure 13 also illustrates that for each frequency below the LHR frequency there is an angle at which perfect transmission occurs regardless of slab thickness. (It happens when $\gamma = 1$ -- Eq. (19) -- i.e., when the ratio E_x/E_y is the same in both media.) This phenomenon is still unexplained. It does not appear to be the usual Brewster angle [Ramo et al., 1965] effect since in the present case the electric field of the wave is not polarized in the plane of incidence.

Finally, for frequencies corresponding to Figure 14c there exists a range of angles for which no real solution of Snell's law exists in the slab. Due to the finite thickness of the slab some tunneling may be expected to occur. However, assuming that the slab is several wavelengths thick, it becomes very strongly reflecting. The behavior of the 10 kHz lines in Figure 13 aptly illustrates this phenomenon.

B. COMPUTATIONAL RESULTS

The simplest and perhaps most instructive model for the banded

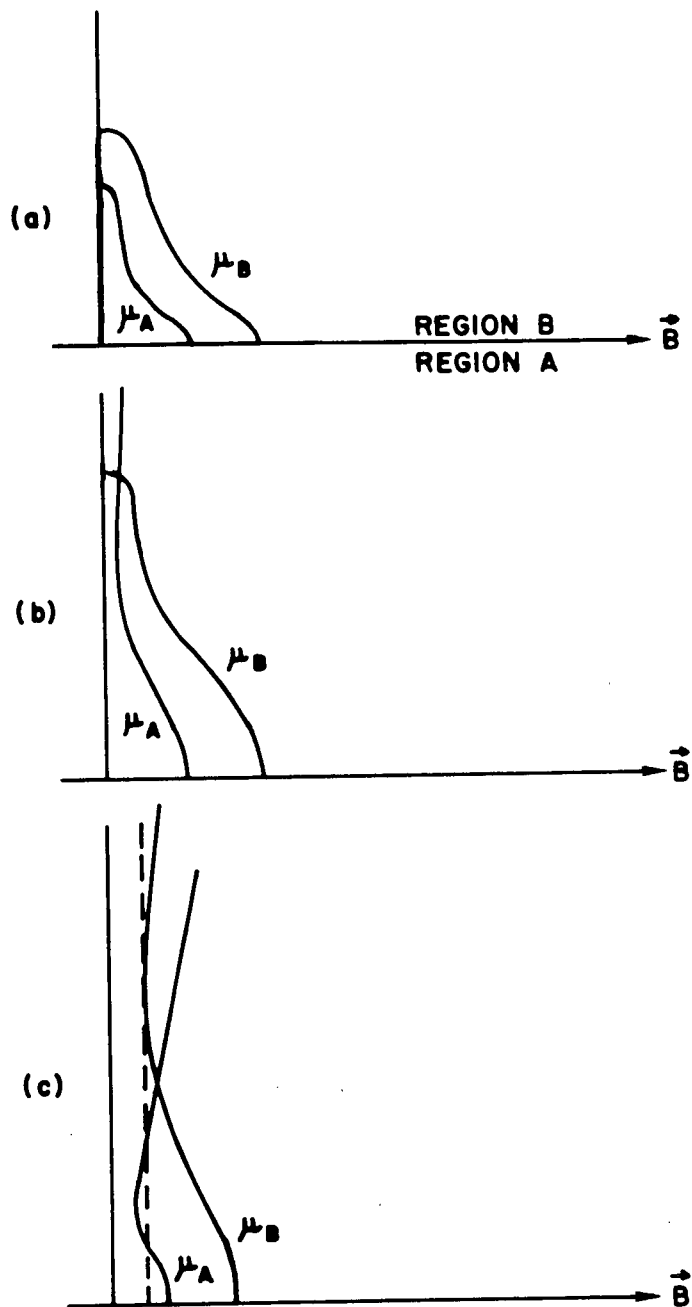


FIGURE 14. SKETCH OF REFRACTIVE INDEX SURFACES μ_A AND μ_B FOR MEDIA A AND B RESPECTIVELY. a) At frequencies below the lower hybrid resonance (LHR) both surfaces are closed. b) At frequencies above the LHR in region A but below that in region B the surface in region A opens and intersects that of region B. c) At frequencies above the LHR in both regions both surfaces are open and intersect. As indicated by the dotted line there is a range of incident wave normal angles for which no solution in region B exists. (For clarity these drawings are not to scale.)

whistler phenomenon is to assume that waves of all frequencies are incident upon the slab at the same wave normal angle. First, note that expression (14) for $|\tau|^2$ maximizes whenever $|\sin(k_{zB}L)| = 0$ that is

$$f \mu_B(f, \theta_B) \sin \theta_B = \frac{mc}{2L} \quad m = 1, 2, \dots \quad (21)$$

For sufficiently small values of θ_B , we may express the refractive index in the quasi-longitudinal (QL) approximation (see Helliwell [1965]). Then, $\mu^2 \sim X/Y \cos \theta$. Thus the lefthand side of Eq. (21) will vary as \sqrt{f} implying that f is proportional to m^2 . This means that the transmission maxima (or reflection minima) will get progressively farther apart as f increases. At the other extreme, let us assume that the constant angle θ_B is so large that it is near the resonance cone angle corresponding to a frequency of 10 kHz. Then as $f \rightarrow 10$ kHz, $\mu_B \rightarrow \infty$. Thus, the successive frequency solutions of Eq. (21) get progressively closer together. It then becomes intuitively plausible that somewhere between these two extremes there will exist angles that will produce a relatively uniform spacing. Figure 15 shows the variation of reflection coefficient with frequency for an incident wave normal angle of 80° , and it confirms the above expectation.

Recognizing the highly idealized nature of this model, let us examine some of its consequences. First, and perhaps most important, the maxima in Figure 15 are much broader than the minima. This differs radically from the spectral amplitude variations predicted by some of the models discussed earlier, and it is in agreement with the spectral shapes observed on many banded whistlers such as the one in Figure 1.

However, this model cannot account for spectra such as that in

whistler 'A' of Figure 3. As indicated above, small incident wave normal angles cause a progressive increase in the spacing of the maxima, large angles produce a decrease, and a small range of intermediate angles produce a relatively uniform spacing. There are no angles at which highly irregular spacings occur.

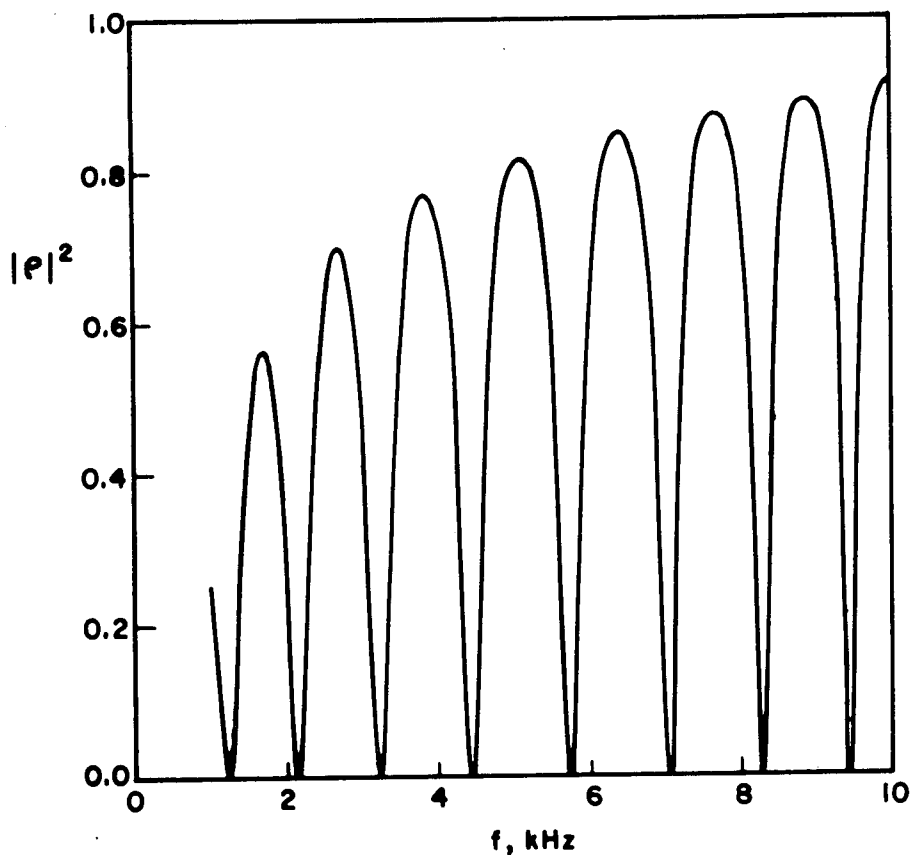


FIGURE 15. REFLECTION SPECTRUM. The variation of the reflection coefficient with frequency is shown. The ambient plasma has one ion (O^+) a plasma frequency of 3.2 MHz, and an electron gyrofrequency of 1.3 MHz. The slab has a density five times ambient and a thickness of 0.35 km. Waves at all frequencies are assumed to be incident at an angle of 10° from the normal to the slab.

Finally, at high wave normal angles, Figure 13 indicates that large density enhancement factors (say ≥ 5) would be required to produce the observed attenuations of ~ 14 db in the transmitted spectra. If we are dealing with reflected spectra, then the situation is slightly different. While large attenuation is easily obtained (the reflected signal amplitude goes to zero when Eq. (21) is satisfied), the problem now is how to reflect enough of the wave to produce a reasonably strong signal without requiring large enhancement factors. While irregularities of this size are known to exist in the auroral regions [Lund et al., 1967] no such variations have been reported at the latitudes where banded whistlers occur. In fact, most observers (see the review article by Calvert and Warnock [1969]) report variations normally on the order of a few percent at midlatitudes.

In summary the assumption that waves of all frequencies are incident on the slab at the same angle requires first, large wave normal angles, and second, high density enhancement factors in order to account for a whistler such as that in Figure 1. However, this assumption is not necessary, and is probably not even tenable. At the very least different frequencies are refracted by different amounts upon entering the ionosphere with the spread in angles proportional to the square root of the frequency. However, for a plasma frequency of 3 MHz and electron gyrofrequency of 1 MHz this will only produce a maximum angular spread on the order of 1-2 degrees in the frequency range of 1-10 kHz. Horizontal gradients may act to increase this spread.

The objections raised in the preceding three paragraphs can be considerably reduced or eliminated by using much smaller incident wave normal angles that are however strongly frequency dependent. This latter

assumption appears to be quite reasonable. For example, ray tracing calculations by Scarabucci [1969] have indicated that the various frequency components of a 1-hop whistler must have a large variation in wave normal angles in order that they all be able to focus on a given satellite position. Rough calculations based on his Figures 45 and 49 indicate a rise on the order of some 30° in the wave normal angles with respect to the earth's magnetic field for a 1-hop whistler at 120 km altitude in the frequency range of 2-10 kHz with sharp drop-offs above and below this range. The variation could be modeled either by a saw-tooth or a sine curve. It must be borne in mind that Scarabucci's results were highly dependent on his assumption of a model for electron density variation. Nevertheless, it appears reasonable to conclude that the wave normal angle of a wave component is highly dependent on its frequency.

A variety of models for the variation of the incident angle θ_I with f were tried. Figure 16 illustrates a highly irregular transmission spectrum. Note the qualitative resemblance to whistler 'A' in Figure 3. Figure 17 shows a reflection spectrum for the same slab, but with a different model for $\theta_I(f)$. Note the exceptionally uniform spacing of the nulls in this spectrum. There is, of course, nothing unique about this model.

The procedure for reproducing a particular banded whistler's spectrum is relatively straightforward once the plasma parameters (i.e., slab location) f_p and f_H have been selected. Using the QL approximation, calculation of the wavelength in the slab (using a "reasonable" value for the enhancement factor, δ) allows calculation of a fairly good estimate for the thickness L which will produce a spacing that

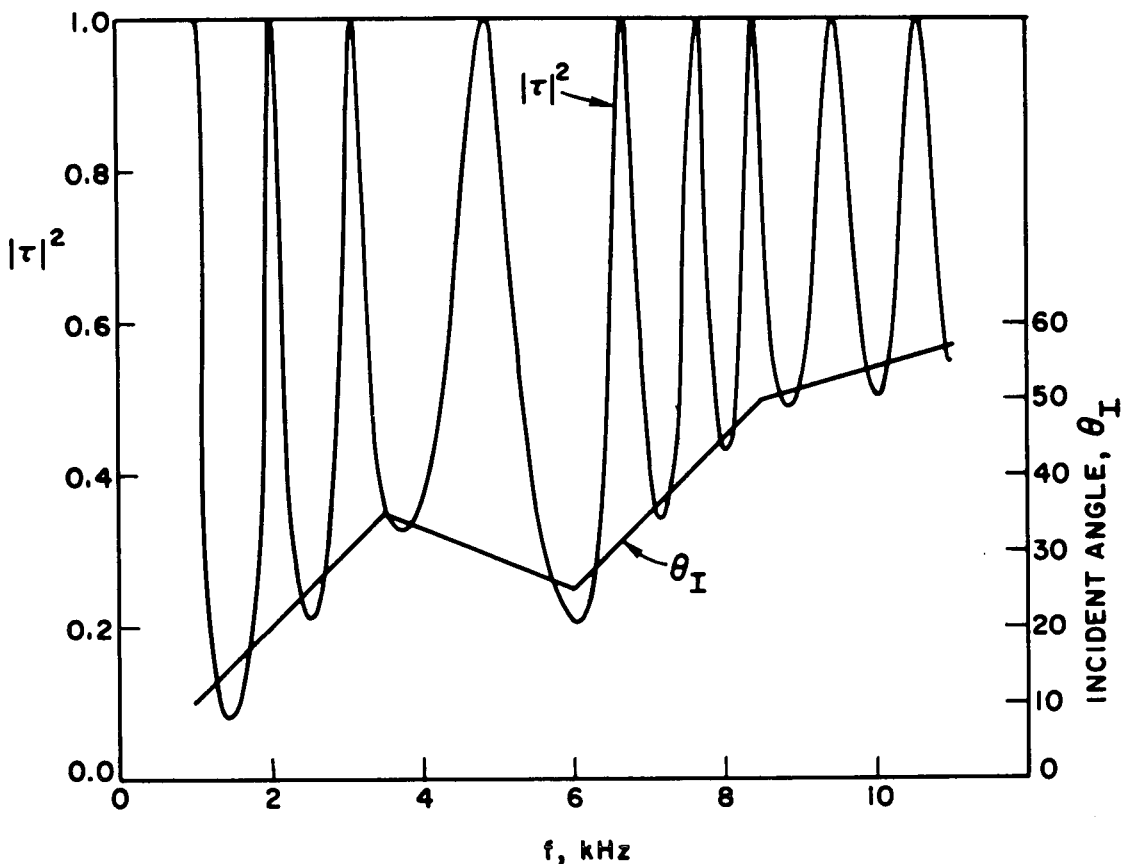


FIGURE 16. COMPUTED TRANSMISSION COEFFICIENTS. The ambient plasma has one ion (O^+), plasma frequency of 3.2 MHz, and electron gyrofrequency of 1.3 MHz. The slab has 2.0 km thickness and a density twice that of the ambient. The variation of incident wave normal angle θ_I with frequency shown above produces an irregular spacing of the maxima. Note how the peaks first have a spacing of ~ 1 kHz, then ~ 1.8 kHz, then ~ 1 kHz again.

will on the average approximate that observed in the whistler. A computer run (taking ~ 2 seconds) assuming that the incident angle θ_I increases linearly by 30° over the 1-10 kHz interval is made. From the results L

may be adjusted if the initial average spacing is too far off. Then adjustments are made to $\theta_I(f)$ bearing in mind that increasing $\theta_I(f)$ in a given frequency interval acts to decrease the spacing between nulls in that range and vice-versa. Figure 17 illustrates a calculated reflection spectrum in which a very uniform spacing between minima was obtained by suitable variation of incident wave normal angle θ_I with frequency. If amplitude information on the whistler is available to be matched, small changes in δ will not affect the calculated spectral shape if the product $L \delta$ is held fixed.

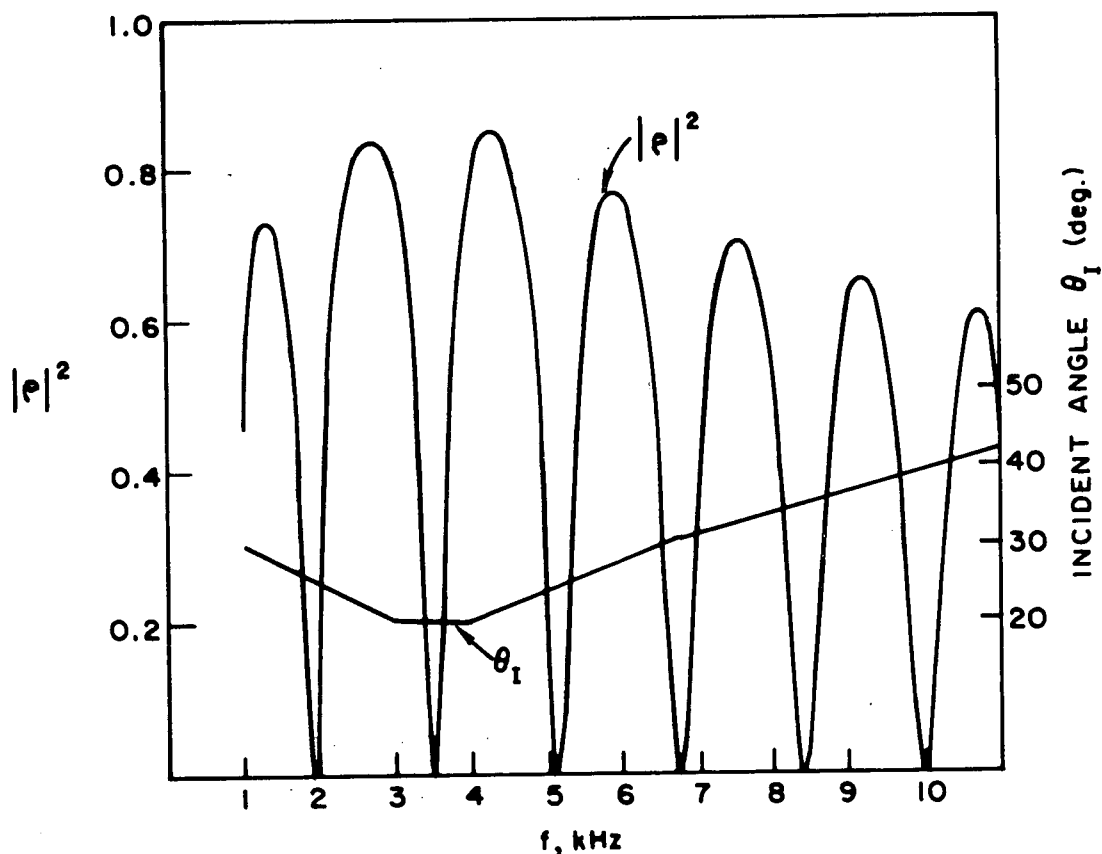


FIGURE 17. COMPUTED REFLECTION COEFFICIENTS. With the same parameters as in Figure 16, but with a different variation of incident wave normal angles with frequency, a very uniform spacing of ~ 1600 Hz is produced.

The exact details of how the wave arrives at the slab and what the actual dependence of θ_I on frequency is require more detailed ray tracing calculations. Two plausible models are schematically illustrated in Figure 18.

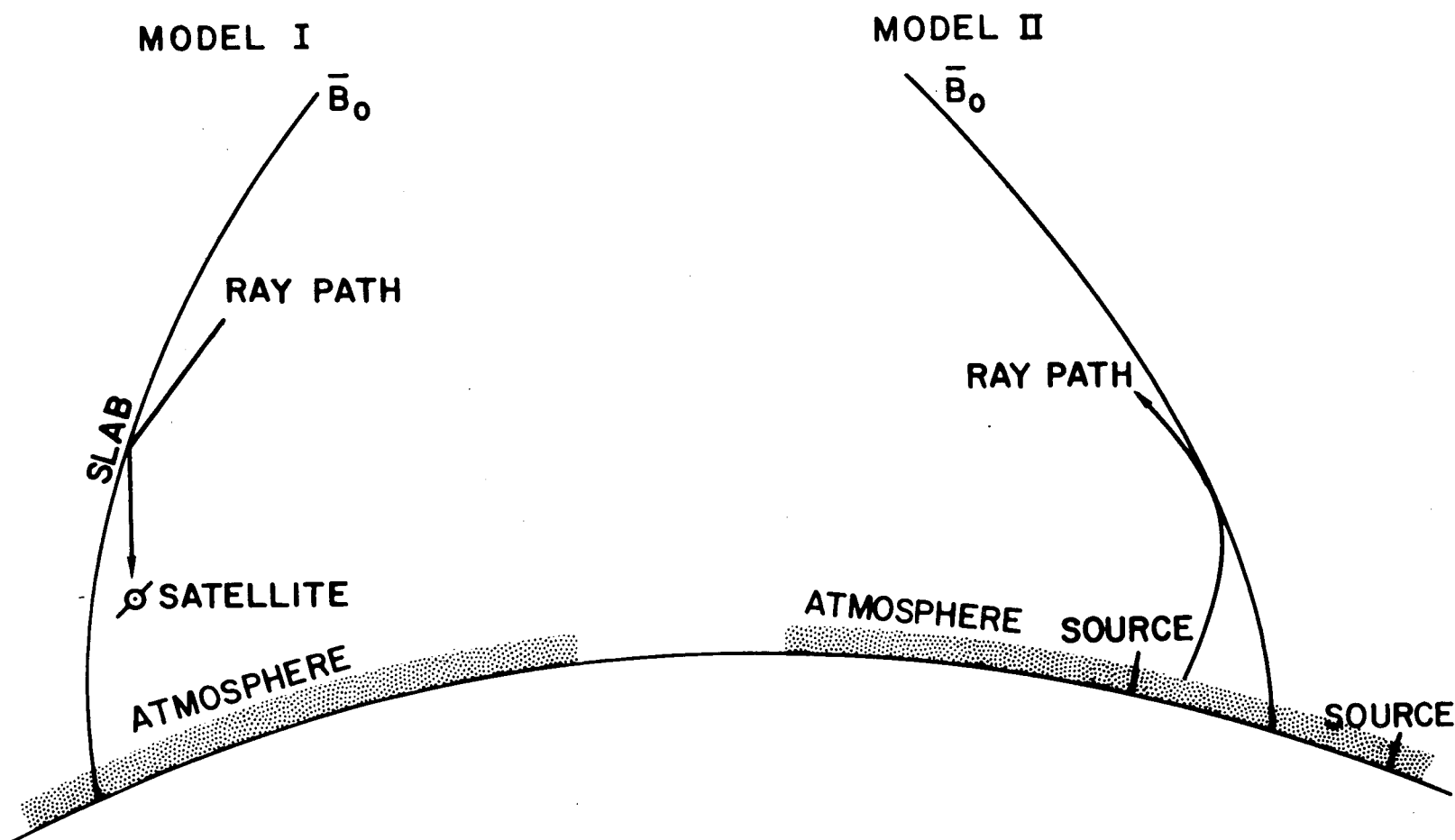


FIGURE 18. TWO WAVE-SLAB INTERACTION MODELS--MODEL I APPEARS TO BE USABLE ON ALL 1-HOP BANDED WHISTLERS. Model II is required for O^+ banded whistlers. It can only produce monotonically varying spacing on 1-hop whistlers. With small enhancement factors and small wave normal angles it can easily reproduce a uniform spacing. Transmission is, of course, also possible for both models. Interaction from the outside of the field line is considered less likely since waves tend to head outward toward higher L values.

IV. DISCUSSION

In the previous chapter several possible mechanisms to explain the banded whistler phenomenon were examined. Only the wave-slab interaction model provided positive results in terms of explaining the observed spectral shapes of the banded whistlers.

This model may also find application in explaining the phenomena shown in Figures 2a and 2b. For example, if the slab were not sharp sided, the ratio of maxima to minima in the spectrum can be expected to reduce. We might well expect to obtain spectra resembling that in Figure 2b.

If this mechanism is indeed the correct one, then it may provide us with a valuable tool for studying some types of ionospheric irregularities. More data should be examined to determine how the banded whistlers (and, by implication, the irregularities) vary with magnetic storm activity (preliminary results indicate that little, if any, correlation exists) and local time.

A particularly good correlation already appears to exist with the data on HF and MF ducting. In a rocket-borne HF sounding experiment Knecht et al., [1961] reported irregularities with thicknesses of about 1 to 10 km. Loftus et al., [1966] using the Explorer 20 topside-sounder found thicknesses ranging from 1 to 40 km. Average thicknesses of 0.6 km were observed by Muldrew [1963] using Alouette 1 data. These are consistent with the thicknesses used in the preceding chapter. In addition, Ramasastry and Walsh [1969] report that ducting is seen up to regions near the plasmapause (while Muldrew [1967] reports that the ducts cut off at $L = 1.3$ to 1.4) which are consistent with the data in Chapter 2.

Another avenue for further research is to improve the rigor of the calculations in the preceding chapter. For completeness, the non-whistler mode should also be included in Eqs. (4) through (7) (providing four new variables) and the conditions for continuity of magnetic fields across di-electric boundaries should be used (thus providing the necessary two new equations at each boundary). For the frequencies of interest in this report, these waves are evanescent, decaying exponentially with distance away from the slab boundaries where they may be excited. To say that these waves are identically zero or have zero "skin depth" [Ramo et al., 1965] is equivalent to saying that the medium behaves like a perfect conductor to this mode and is thus capable of supporting surface currents. In the presence of surface currents the tangential \vec{B} fields are not continuous across the surface. Thus the choice of continuity of \vec{E} rather than \vec{B} fields in Eqs. (4) through (7) seems consistent with the assumption that the non-whistler mode waves could be neglected. Hence, we can see that this assumption has profound mathematical implications. However, from the physical point of view, it is not expected that the greatly increased mathematical complexity which will result from relaxing this assumption will significantly change the results because these extra waves are nonpropagating.

It should also be noted that Eq. (8) ignored collisions. This is justified by the fact that the collision rate, which is of order 10^2 at satellite altitudes, is small compared with the whistler frequencies.

In summary, the mechanism of spectral reflection or transmission from a field aligned slab of enhanced ionization appears to be best able to explain the observed spectral shapes of the banded whistlers. The

model assumes that the slab's density is much larger (at least by a factor of two) than that of the ambient plasma. Since such irregularities have not yet been reported in the literature as having been seen at the mid-latitudes where the banded whistlers occur, this assumption must stand as a prediction of the model.

APPENDIX

```

PROGRAM SLAB
REAL MASS
DIMENSION F(500),T(500)
COMMON MASS,FP,FH,WR,WL,WE,W0
PI=3.1415926526
RAD=PI/180.
MASS=29376.
FP=3200000.
FH=1300000.
DELTA=1.5
ANGLE=16.
THKNS=4.
F(1)=1000.
PRINT 510
510 FORMAT(' FREQUENCY  ANGLE  REFLECTION COEFFICIENTS',/ ' <H7')
DO 500 J=1,201
C*** CALCULATE THE SQUARE OF THE PHASE VELOCITY IN THE AMBIENT PLASMA
PHI=P(I,F(J),ANGLE ,PI,RAD)
CALL FORMOD(F(J))
A=(WE-W0)*SIN(PHI)**2
W1=WE-.5*A+SQRT(A*A+((WR-WL)*COS(PHI))**2)*.5
IF(W1) 502,502,450
450 POLAR1=2.*TAN(PHI)*(WE-W1)*(W0/W1)/(WR-WL)
C*** CALCULATE THE SQUARE OF THE PHASE VELOCITY IN THE SLAB
FP=FP*SQRT(DELTA)
CALL FORMOD(F(J))
FP=FP/SQRT(DELTA)
D=COS(PHI)**2/W1
A=1.-D*WE+D*W0
B=D*(WR*WL-WE*W0)-W0-WE
BB=B*B-4.*A*W0*WE
IF(BB) 502,470,470
470 W2=.5*(-B+SQRT(BB))/A
IF(W2*D-1.) 490,490,522
490 PHI2=ARCOS(SQRT(W2*D))
C*** CALCULATE THE REFLECTION COEFFICIENT
X=((TAN(PHI2)*2.*(WE-W2)*(W0/W2)/(WR-WL))/POLAR1)**2
WAVE=1.5E5*SQRT(W2)/(F(J)*PI*SIN(PHI2))
A=SIN(THKNS/WAVE)**2
T( J)=1.-4.*X/(4.*X*(1.-A)+A*(1.+X)**2)
601 IF(J-1) 600,600,501
600 WAVE=2.*WAVE*PI
501 CONTINUE
E=PHI/RAD
PRINT 512,F(J),E,T(J)
512 FORMAT(' ',F10.0,F6.2,F16.6)
500 F(J+1)=F(J)+50.
502 PRINT 603,WAVE
603 FORMAT(' WAVELENGTH AT 1 KH7 IS ',E16.6)
STOP
END

```

Reproduced from
best available copy.

```

SUBROUTINE FORMOD(F)
C**** THIS ROUTINE COMPUTES THE SQUARE OF THE PHASE VELOCITIES OF THE
C**** LIMITING MODES IN A ONE ION PLASMA. WR AND WL REPRESENT THE
C**** VALUES AT ZERO DEGREES OF THE FAST AND SLOW MODES RESPECTIVELY.
C**** SIMILARLY, WE AND WD ARE THE RESPECTIVE VALUES EVALUATED AT
C**** NINETY DEGREES.
REAL MASS
COMMON MASS,FP,FH,WR,WL,WE,WD
X=(FP/F)**2
Y=FH/F
WR=1./((1.-X*(MASS+1.))/((1.-Y)*(MASS+Y)))
WL=1./((1.-X*(MASS+1.))/((1.+Y)*(MASS-Y)))
WD=1./((1.-X-X/MASS))
WE=((1.+X*(MASS+1.)*(Y*Y-MASS))/((Y*Y-1.)*(Y*Y-MASS**2)))*WR*WL
RETURN
END

```

```

FUNCTION P(I,G,H,PI,RAD)
C**** THIS ROUTINE COMPUTES THE VALUE OF THE INCIDENT ANGLE,P, AS A
C**** FUNCTION OF THE FREQUENCY,G, AND THE INCIDENT ANGLE AT 1 KHZ,H.
IF(G-4000.) 1,1,2
1 P=(H-(G-1000.)/200.)*RAD
RETURN
2 IF(G-6500.) 3,3,4
3 P=(H-15.+(G-4000.)* 7./2500.)*RAD
RETURN
4 P=(H- 8.+(G-6500.)*12./4500.)*RAD
RETURN
END

```

REFERENCES

- Brice, N. M. and R. L. Smith, Lower hybrid resonance emissions, J. Geophys. Res., 70, 71, 1965.
- Calvert, W. and J. M. Warnock, Ionospheric irregularities observed by topside sounders, Proc. IEEE, 57, 1019, 1969.
- Gurnett, D. A. and S. R. Mosier, VLF electric and magnetic fields observed in the auroral zone with the Javelin 8.46 sounding rocket, J. Geophys. Res., 74, 3879, 1969.
- Helliwell, R. A., Whistlers and Related Ionospheric Phenomena, Stanford University Press, Stanford, California, 1965.
- Knecht, R. W., T. E. VanZandt and S. Russell, First pulsed radio soundings of the topside of the ionosphere, J. Geophys. Res., 66, 3078, 1961.
- Loftus, B. T., T. E. VanZandt, and W. Calvert, Observation of conjugate ducting by the fixing-frequency topside-sounder satellite, Ann. Geophys. 22, 530, 1966.
- Lund, D. S., R. D. Hunsucker, H. F. Bates, and W. B. Murcay, Electron number densities in auroral irregularities, comparison of backscatter and satellite data, J. Geophys. Res., 72, 1053, 1967.
- Muldrew, D. B., Radio propagation along magnetic field aligned sheets of ionization observed by the Alouette 1 topside sounder, J. Geophys. Res., 68, 5355, 1963.
- Muldrew, D. B., MF conjugate echoes observed on Alouette 2 topside sounder data, Canad. J. Phys., 45, 3935, 1967.
- Ramasasthy, J. and E. J. Walsh, Magnetospheric duct propagation research using Alouette 2 topside sounder observations, NASA TN D-5332,
- Ramo, S., J. R. Whinnery and T. Van Duzer, Fields and Waves in Communication Electronics, John Wiley and Sons, New York, 1965.
- Rorden, L. H., L. E. Orsak, B. P. Ficklin and R. H. Stehle, Instruments for the Stanford University/Stanford Research Institute VLF experiment on the EOGO satellite, Instr. Rept., Stanford Research Institute, Menlo Park, California, May 1966.
- Scarabucci, R. R., Interpretation of VLF signals observed on the OGO-4 satellite, Tech. Rept. No. 3418-2, Stanford Electronics Labs., Stanford University, Stanford, California, October 1969.
- Shaw, R. R. and D. A. Gurnett, Whistlers with harmonic bands caused by multiple stroke lightning, J. Geophys. Res., 76, 1851, 1971.

Smith, R. L., Magneto-ionic theory with ions and electrons, Class notes for EE 275, Stanford University, Stanford, California, Jan. 1968.

Smith, R. L. and N. Brice, Propagation in multi-component plasmas, J. Geophys. Res., 69, 5029, 1964.

Storey, L. R. O., An investigation of whistling atmospherics, Phil. Trans. Roy. Soc. (London) A, 246, 113, 1953.

Thorne, R. M., Whistler mode propagation off the geomagnetic meridian plane, Dept. of Meteorology, UCLA, Los Angeles, Calif., Feb. 1969.

Uman, M. A., Lightning, McGraw-Hill, Inc., New York, 1969.